Follow-the-leader motion simulation of a continuum manipulator with linear curvature segments

S.C.A. Vieveen

MSc Thesis report

Daily supervisor

Ir. C. Culmone

Supervisors

Prof. Dr. Ir. P. Breedveld

Ir. P.W.J. Henselmans

Dr. Ir. M. Langelaar

Date: 17-01-18

Abstract

Background: Delft University of Technology has developed two working prototypes of flexible instruments for surgery, together with a master-slave system. The master-slave system is compatible with the simple parallel cable configuration and the more complex parallel and diagonal cable configuration. It is assumed that the instrument with a complex cable configuration requires fewer segments, compared to an instrument with a simple cable configuration, to cover a complex path, with the same accuracy.

Study design: research

Methods: The two different cable configurations are modeled. The model will first determine the shapes one segment can form. Afterwards, the possible shapes of the segments are combined to judge the performance of the flexible instruments with an algorithm. The algorithm is purely kinematic and does not take forces into account.

Results: The results show a strong preference for the cable configuration with parallel and diagonal cables. This configuration needs fewer degrees of freedom to reach the same error.

Conclusion: Therefore it can be concluded that the cable configuration with parallel and diagonal cables is more promising in combination with the predesigned master-slave system.

Acknowledgments

The creation of this thesis would not have been possible without the support of my family and friends my daily supervisors and my main supervisor at the TU Delft. Therefore I would firstly like to thank my parents for their support and patience throughout my study. Their supportive advice and patience to listen. I would also like to thank my girlfriend for her support time and her encouragement.

A special thanks go out to my daily supervisor Paul Henselmans for his input feedback and vision throughout the design of my thesis. I would also like to thank Constanza Culmone, as my daily supervisor later in the project, for the support and critical reading.

Furthermore, I would like to thank Paul Breedveld and Mathijs Langelaar for the intensive feedback at the last part of the project.

Finally, I would like to thank my friends that support me during the creating of my thesis. A special thanks goes out to; Tom Noë, Ruben Verhoef, Ricardo Rinsma, Robin Bolder, Thomas Overklift and Kyle de Jonge.

Table of Contents

1. Introduction 1

1.1 Instrumentation 1

1.2 Problem statement and goal 3

1.3 Method 4

1.4 Contents 4

2. Modelling of a segment 5

2.1 Cable configuration 5

2.2 Force and moment analysis 6

2.2.1 Parallel cables 6

2.2.2 Diagonal cables 7

2.2.3 Parallel and diagonal cables 8

2.3 Multiple segments 9

2.4 Shape investigation 10

2.4.1 Premises 10

2.4.2 Shape deformation 12

2.5 Non-Linearity 13

2.6 Possible shapes 14

3. Kinematic simulation of multiple segments 16

3.1 Path optimizing 16

3.2 Shape determination 18

3.3 Calculation structure 19

3.3.1 Desired path for the simple and complex segments 19

3.3.2 Global and local frames 20

3.3.3 Simple segment calculation 21

3.3.4 Complex segment calculation 22

3.3.5 Error calculation 24

3.3.6 Validation 26

4. Case studies 27

4.1 Case 1 straight 27

4.2 Case 2 exponential 28

4.3 Case 3 sinusoid 28

4.4 Case 4 circular arcs 29
4.5 Performance evaluation 30
5. Results and analysis 32
5.1 Case 1 straight 32
5.2 Case 2 exponential 34
5.2.1 Case 2.1 34
5.2.2 Case 2.2 36
5.3 Case 3 sinusoid 38
5.3.1 Case 3.1 38
5.3.2 Case 3.2 40
5.4 Case 4 circular arcs 42
5.4.1 Case 4.1 42
5.4.2 Case 4.2 44
5.5 Overview of the results 46
6. Discussion 50
6.1 Information 50
6.2 Limitations of the model 51
6.3 In practice 51
6.4 Design recommendations 52
6.5 Future recommendations 52
7. Conclusion 53
8. Literature sources 54

1. Introduction

Minimally invasive surgery has become the new standard in the field of surgery [1]. This way of operating minimizes the size of the incisions and the technique brings other advantages. Less invasive surgical operations reduce postoperative pain, the amount of scar tissue and the recovery time [2-8]. Moreover, the reduced recovery time decreases the hospital cost drastically [2, 3, 5-7]. It is a trend in surgery to minimize the number and the size of incisions since the first introduction of laparoscopy [2, 9-11]. The technical developments in surgical instruments are one of the drivers for this new way of operating [9,12].

The least invasive manner of operating is via natural orifices, this is called Natural Orifice Transluminal Endoscopic Surgery. This way of operating introduces benefits on top of the benefits of MIS, mainly, improved cosmetics, reduced systematic inflammatory response and a reduction in postoperative pain [13]. However, in practice NOTES is still in its infancy.

1.1 Instrumentation

Modern instrumentation provides the possibility to enable and enhance performance in MIS. However, to export these benefits to areas that require a more delicate circuitous access is challenging. Numerous procedures can still only be approached with open surgery. ‘’Thus, it would be greatly beneficial to have manipulators which are scalable to a small size, flexible yet strong, and which can reach difficult-to-access surgical sites via nonlinear pathways and complete the surgical task with dexterity.’’ [12]

Skull-base surgery is one example of a complicated anatomy for operations. A schematic representation of skull-base surgery is shown in Figure 1. Instead of using open surgery, the procedures are slowly evolving to a less invasive endoscopic endonasal approach [14]. However, the possibilities of endonasal operations are limited due to the current instruments that lack maneuverability [14]. Therefore, more flexible instruments are needed.

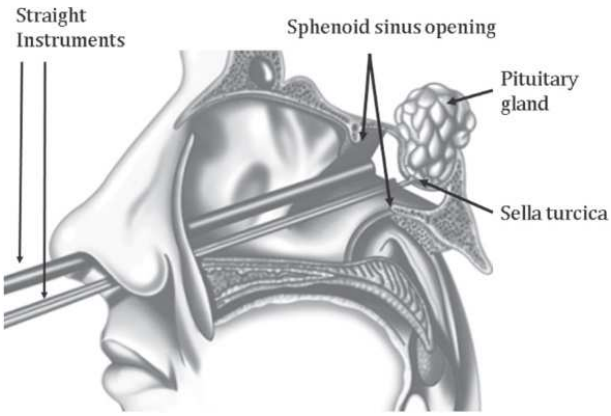

Figure 1: A schematic representation of skull base surgery [14].

There are already flexible instruments on the market, bronchoscopes and colonoscopes for instance. Although these instruments are flexible, they cannot be used for the more complicated surgery sides, because they are not self-supportive, and require support and guidance from the environment. While delicate tissue, for instance at the skull base, is not capable of providing this kind of support, due to a high number of small blood vessels, nerves and other types of fragile tissue.

There is need for small size, flexible yet stiff instruments, which can move across non-linear pathways. Several research groups came to this conclusion. Therefore, a number of flexible instruments are currently in development.

One of the most famous flexible instruments is HARP. HARP is a flexible instrument consisting of two concentric tubes, one outer and one inner

tube [15]. These tubes are able to alternate between a rigid and a limp state. Whenever the inner tube is rigid and the outer tube is limp, the outer tube can slide over the inner tube, and moves forward while being steered. Afterwards, the outer tube is made rigid and the inner tube is made limp, so the inner tube can follow.

Despite the fact that HARP is an instrument capable of following a complex path, it is 12 mm thick and therefore too large for endonasal skull base surgery. The diameter of the instrument is also hard to scale down because the system is friction based. Reducing the diameter will increase the tension in the material, causing it to deform plastically.

For this reason, the Technical University of Delft is developing its own flexible instruments and a matching shape memory system to control them. This shape memory system consists of a desired physical track, a master and a slave. The master follows a physical track ex vivo. This master consists of the same segments as the slave. The master is pushed over the physical track and is therefore forced to follow the physical track. The slave is controlled by the master and follows the movement of the master track in vivo. The slave is controlled by cables. These cables are only attached at the end of each segment. Therefore, it is only possible for the master to prolong the angle and position at the end of each segment to the slave. In Figure 2 the green track is the predefined physical track that the master follows, while the blue track is the track which the slave will make due to the control of the master.

The master and slave can be connected via different cable configurations. The Technical University of Delft has developed two different prototypes of flexible instruments with different cable configurations.

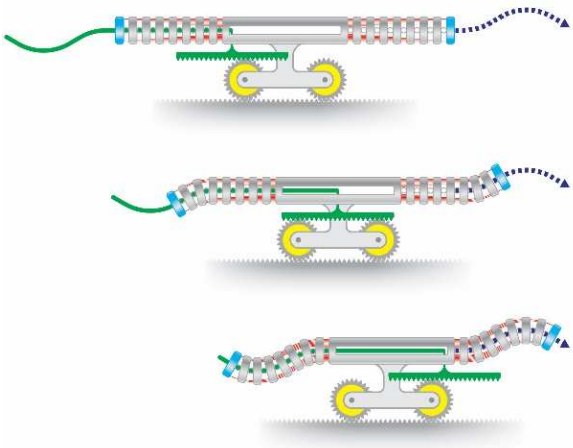

Figure 2: A schematic representation of the master-slave system. [16]

The first prototype is called the Multiflex, see Figure 3. This instrument consists of multiple segments. These segments have one degree of freedom, also referred to as DOF, and are cable controlled. The cables are positioned parallel among the shaft of the instrument. Each segment is capable of forming an arc with a constant curvature. Due to the configuration of the cables, it is only possible to adjust the angle of the tip of a segment, so only the angle is provided from the master to the slave.

The second one has a more complex cable configuration and is called the Helixflex, see Figure 4. This instrument is comparable to the Multiflex. The main differences are in the number of segments and in the cable configuration. The Helixflex has parallel and diagonal cables. The instrument has only one segment, and this segment has two DOF. Therefore, the segment is capable of forming more complex shapes. This makes it possible to control the position and angle of the tip of a segment.

Figure 3: An image of the tip of the Multiflex. [17]

Figure 4: An image of the tip of the Helixflex. [14]

These two different cable configurations both have their advantages and disadvantages. However, it is inefficient to develop two different instruments with the same purpose. Thus the question is: "Which of the two cable configuration is more promising and therefore should be used for further developments?".

To answer this question there is taken a look at algorithms to define the maneuverability of flexible instruments. For the navigation of flexible instruments, there are already multiple existing algorithms such as path planning and the avoidance of particular obstacles. Chirikjain et al. developed a planar obstacle avoidance algorithm [18]. The algorithm gave a discrete solution towards an imaginary instrument. This instrument was capable of forming any continuous line, although the length was predefined. Choset and Henning [19], extended the version of Chirikjain et al. by adding a follow the leader approach.

A.A. Maciejewski et al. and I.S. Godage et al. also show an obstacle avoidance algorithm for rigid robots J. Burgner et al. applies this algorithm to continuum robots [13, 20, 21].

However, the control of the Multiflex and Helixflex works with a desired physical track, as described previously. Besides, the master that retrieves the information from the physical track has its limitations. It should be taken into account that the master can only retrieve information at the end of each segment. The cables transmit the information. The amount of information that can be transmitted depends on the cable configuration. A configuration with two cables can only transmit an angle at the tip of the segment, while a configuration with four cables can transmit an angle and a position.

The preformed track will deliver endpoints and angles to each segment of the master. These endpoints and angles are the information that the master reads from the preformed track. That information is provided to the slave by the cables. This method is different than the other described algorithms because it is based on a real instrument together with its restrictions, where other algorithms are often based on imaginary instruments. It was decided to compare two cable configurations, based on the Multiflex and Helixflex, with the use of a specific path planning method based on the input to the instrument. This way the instruments can be compared as objective as possible.

1.2 Problem statement and goal

The Technical University of Delft has developed two working prototypes of flexible instruments, together with a master-slave system. The master-slave system is compatible with the simple parallel cable configuration and the more complex parallel and diagonal cable configuration.

Hypothesis: The instrument with a complex cable configuration requires fewer segments, compared to an instrument with a simple cable configuration, to cover a complex path, with the same accuracy.

This report will examine this statement. This is done by developing an algorithm to compare the maneuverability of both configurations.

1.3 Method

The instruments will be simulated with an algorithm programmed in MATLAB R2016b to compare their maneuverability. Firstly the model of the instruments will define the possible shapes that a segment is able to form. The deformation is calculated and backed up by previous research. Afterwards, those shapes of individual segments are used to investigate the total shape an instrument can form. The algorithm used for this investigation is purely kinematic and does not take forces into account. The performance of an instrument is judged on the ability to overlay different predefined paths.

There is decided for a kinematic algorithm to decrease the complexity of the algorithm. The forces on the cables are rather difficult to calculate. Specifically with the friction forces that depend heavily on the construction and design choices of the instrument. Besides the algorithm is to compare the maneuverability, so the forces on the cables are less interesting.

There are multiple reasons to calculate the maneuverability of the instruments with an algorithm, instead of a test with the prototypes. The first reason is the adjustability of code. The number of segments and the length of the segments of the prototypes cannot easily be adjusted. The algorithm can, however, be adjusted easily.

The second reason is that the produced prototypes are not compatible with the master-slave system jet. Although the concept of the instruments is compatible with the master-slave system, the produced prototypes are not.

A third reason is that an algorithm can investigate the final potential of the instruments, while a prototype test would only show insights in the now produced prototypes. Those results will be based on the limitations of the prototypes, which might be overcomable in the future.

1.4 Contents

Chapter 2, *Modelling of a segment*, models a single segment for both a simple and a complex cable configuration. Chapter 3, *Kinematic simulation of multiple segments*, will investigate the kinematic workspace of multiple segments attached to each other, together with the possibility of following a path. This will be done by programming the kinematic possibilities of one segment in the software program MATLAB. Chapter 4, C*ase studies*, will introduce multiple virtual paths to test the maneuverability of the instruments. Chapter 5, *Results and analysis*, will present the results of the maneuverability tests from the case studies and will compare and interpret these results. Chapter 6, *Discussion*, will discuss the results of the previous chapters and investigates the possible implementations, together with further recommendations. Chapter 7, C*onclusion*, will look back on the problem statement and will conclude the final results of the report.

2. Modelling of a segment

Intro

In this chapter a single segment for different cable configurations will be modeled. The cable configurations are based on the cable configurations of the Multiflex and the Helixflex. Firstly, the cable configurations will be described. Force and moment calculations will follow. Afterwards, the kinematics of the instruments will be discussed. This study will focus on the movement in a two-dimensional frame. This makes it possible to compare the maneuverability while reducing the model's complexity, compared to a three-dimensional model.

2.1 Cable configuration

The basic segment for the cable configurations is displayed in Figure 5. The shaft has a length L, is compliant and is axially incompressible. The ribs are rigid with a total width of 2·R. The cables are attached to top ribs and pass through a sufficient number of cable guides, see Figure 6. Notice that the cable guides are left out in Figure 5. These ribs are used to guide the cables through the segment, the cables are, however, only fixed at the bottom and the top rib.

Possible configurations

Multiple cable configurations are possible. These configurations will directly affect the kinematics of the segment. All the configurations are symmetrical, which results in symmetrical behavior. The configuration that is based on the Multiflex segment is presented in Figure 5a. This segment has two parallel cables and will also be referred to as the simple configuration. Another possible configuration is diagonal cables instead of parallel cables, see Figure 5b. Or a combination of both, based on the Helixflex see Figure 5c. These three different constructions will be investigated.

Parallel cables

The first construction, Figure 5a, has parallel cables. These parallel cables can create a force in the y-direction, parallel to the longitudinal axis of

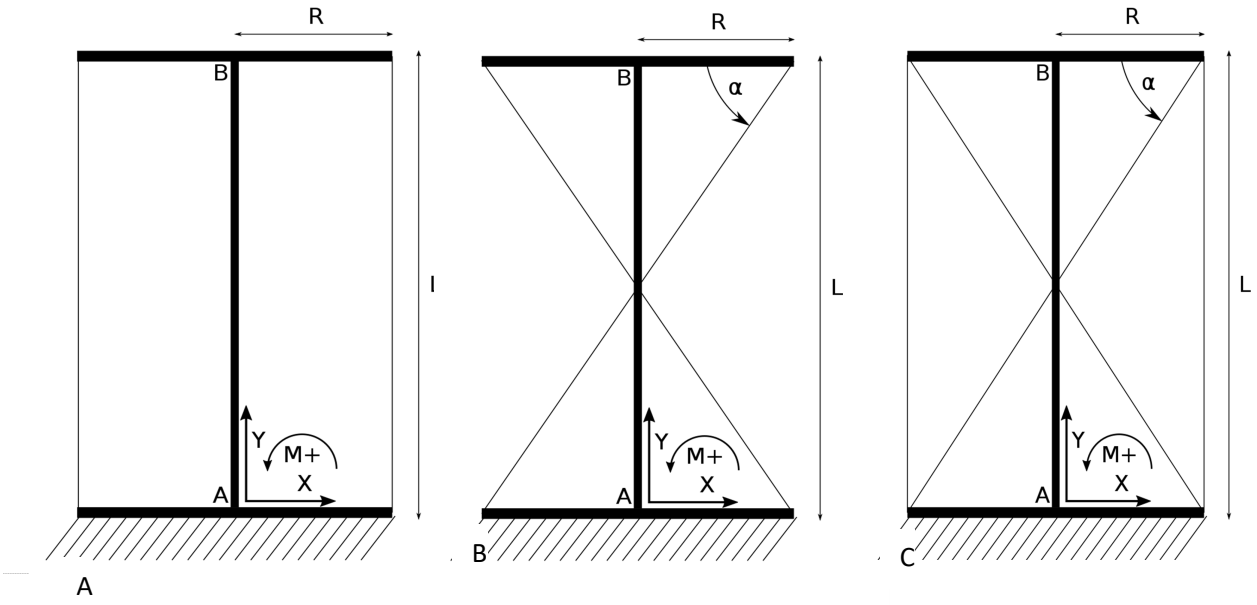

Figure 5a: A schematic representation of a segment with two parallel cables. Figure 5b: a schematic representation of a segment with two diagonal cables. Figure 5c: a schematic representation of a segment with two parallel and two diagonal cables.

the segment, to create a moment around the shaft.

Diagonal cables

The second construction, Figure 5b, has diagonal cables. These diagonal cables can create a force in the direction of the cables. This force can be split into an x- and a y-component.

Parallel and diagonal cables

The third construction, Figure 5c, has parallel and diagonal cables. These parallel cables can create a force in the y-direction. The diagonal cables can create a force in the direction of the diagonal cables.

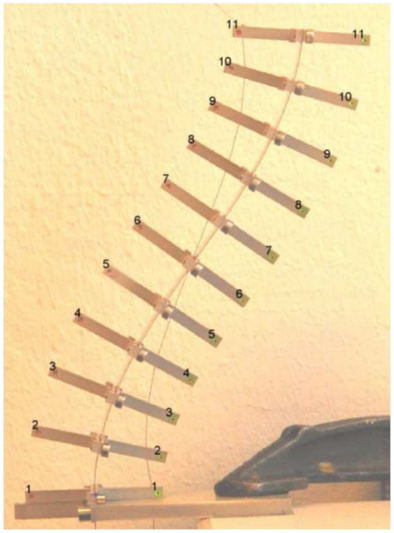

Figure 6: A two-dimensional prototype of one segment with nine cable guides. [22]

2.2 Force and moment analysis

In order to compute the bending of the shaft, the forces in the cables need to be described. First, the segment with parallel cables will be analyzed. Afterwards, diagonal cables and the combination follow.

2.2.1 Parallel cables

One way of positioning the cables is to use parallel cables. The forces will be called left parallel forces F_{lp} and right parallel forces F_{rp}. They only have a y component and are made red in Figure 7. This configuration is based on two cables, so it will only be able to control one DOF.

Force analysis parallel cables

A schematic representation of a segment with parallel cables can be seen in Figure 7. The figure shows a force applied by both cables. These forces can be split into an x- and a y-component.

$$F_x = 0 \qquad (2.1)$$

$$F_y = F_{lp} + F_{rp} \qquad (2.2)$$

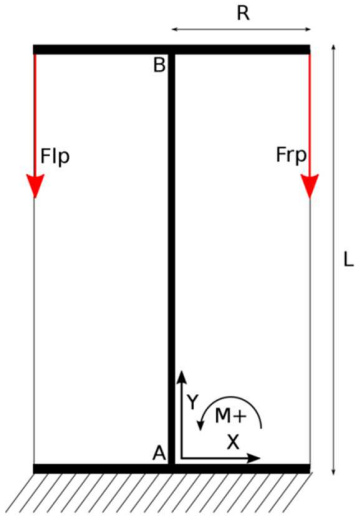

Figure 7: A schematic representation of a segment with two parallel cables, with a force Flp applied to the left cable and a force Frp applied to the right cable.

Moment analysis parallel cables

The moment around the shaft can be calculated with the applied force and the arm of the applied force. The y-component of the parallel force will create a constant moment around the shaft because the perpendicular distance to the shaft stays the same length R. The force in the x direction is equal to zero, therefore it does not influence the moment. The total moment can be calculated with the following equation.

$$M_{total} = R \cdot F_{lp} - R \cdot F_{rp} \qquad (2.3)$$

If the force of the left parallel cable is larger than the force of the right parallel cable the moment would be positive. If it is the other way around the moment would be negative. The moment diagram can be viewed in Figure 8.

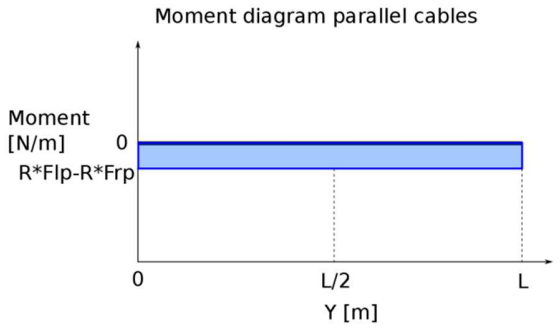

Figure 8: A moment diagram of a segment with parallel cables, both cables apply a force.

2.2.2 Diagonal cables

Another way to position the cables is diagonal. This configuration is also based on two cables, so it will only be able to control one DOF.

Force and moment analysis diagonal cables

The forces are represented in Figure 9. Note, the forces are made red, the green arrows are the horizontal and vertical components of the forces, called F_{lx}, F_{rx}, F_{ly} and F_{ry}. The magnitude of the x and y -components can be calculated with the following equations.

$$F_{lx} = cos(\alpha) \cdot F_l \quad (2.4)$$

$$F_{rx} = cos(\alpha) \cdot F_r \quad (2.5)$$

$$F_{ly} = sin(\alpha) \cdot F_l \quad (2.6)$$

$$F_{ry} = sin(\alpha) \cdot F_r \quad (2.7)$$

The moment around the shaft can be calculated with the following equation:

$$M_{total}(Y) = -(\mathrm{L} - Y) \cdot F_{lx} + \mathrm{R} \cdot F_{ly} + (\mathrm{L} - Y) \cdot F_{rx} - \mathrm{R} \cdot \mathrm{F}_{ry} \quad (2.8)$$

Notice that Y is measured from the bottom of the segment, and determines the moment around a certain point on the shaft of the segment. If Y=L the moment is calculated around B, if Y=0 the moment is calculated around A, and every value in between correspond with a certain point on the shaft between A and B. Equation 2.8 can be simplified to:

$$M_{total}(Y) = R \cdot (F_{ly} - F_{ry}) + (L - Y) \cdot (F_{rx} - F_{lx}) \quad (2.9)$$

Because the ratio between F_{lx} and F_{rx} is the same as the ratio between R and L/2, This can also be substituted to

$$M_{total}(Y) = (L - Y) \cdot F_{rx} - F_{rx} \cdot (L/2) - (L - Y) \cdot F_{lx} + F_{lx} \cdot (L/2) \quad (2.10)$$

This can be simplified to

$$M_{total}(Y) = (L - Y) \cdot (F_{rx} - F_{lx}) - (L/2) \cdot (F_{lx} - F_{rx}) \quad (2.11)$$

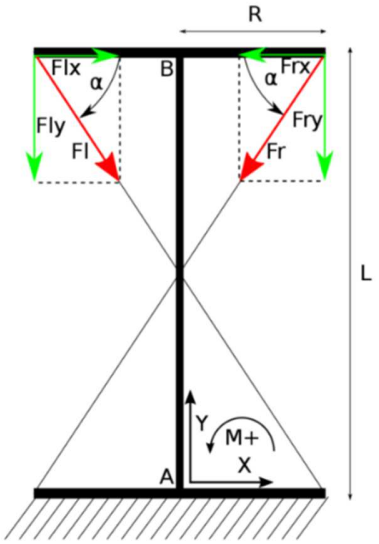

Figure 9: A schematic representation of a segment with two diagonal cables, with a force Fl applied to the left cable and a force Fr applied to the right cable. Notice the x and y components are not defined in the direction of the axis.

The equation 2.11 leads to the conclusion that the moment is zero in the middle of the shaft when y equals L/2. This is always the case and can be easily checked because the diagonal force will have no arm to the center point of the beam. As can be seen in Figure 10, the moment is zero at the center of the shaft. Besides being linear, the moment is also opposed but equal at the start and the end of the shaft.

If the force of the left diagonal cable is larger than the force on the right diagonal cable, the moment diagram will be flipped upside down.

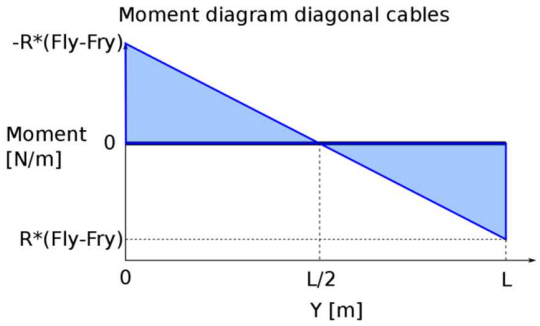

Figure 10: A moment diagram of a segment with diagonal cables, on both cables applies a force.

2.2.3 Parallel and diagonal cables

Both ways of positioning the cables can also be combined into one. This will give the controller of the segment the possibility to adjust the force on four different cables.

Force and moment analysis all cables

If all four cables will apply a force on the construction a linear moment will occur. The moment is an addiction of the moment for parallel cables and the moment for diagonal cables. Figure 11 gives an impression of the forces. The moment around the shaft can be calculated with the following equation.

$$M_{total}(Y) = R \cdot F_{lp} - R \cdot F_{rp} + (L - Y) \cdot (F_{rx} - F_{lx}) - (L/2) \cdot (F_{lx} - F_{rx}) \quad (2.12)$$

This equation is an addition of the moment equation for parallel cables (2.3) and diagonal cables (2.11). The moment diagram is also an addition of both diagrams, see Figure 12. The equation can be simplified to:

$$M_{total}(Y) = R \cdot (F_{lp} - F_{rp}) + (L - Y) \cdot (F_{rx} - F_{lx}) - (L/2) \cdot (F_{lx} - F_{rx}) \quad (2.13)$$

If Y=L the moment is calculated around B and the equation is

$$M_{total}(Y) = R \cdot (F_{lp} - F_{rp}) - (L/2) \cdot (F_{lx} - F_{rx}) \quad (2.14)$$

If Y=0 the moment is calculated around A and the equation is

$$M_{total}(Y) = R \cdot (F_{lp} - F_{rp}) + (L/2) \cdot (F_{lx} - F_{rx}) \quad (2.15)$$

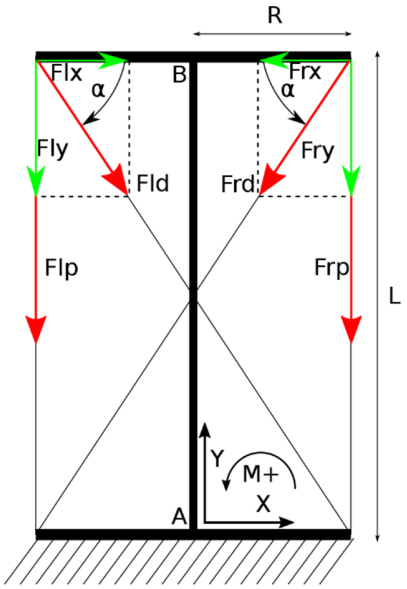

Figure 11: A schematic representation of a segment with two parallel and two diagonal cables, with a force applied on both cables to all cables, where the forces are split into x and y components. Notice the x and y component are not defined in the same direction as the axis.

All three different cable configurations result in different moment distributions along the shaft.

- Parallel cables give the possibility to create a constant moment along the shaft.
- Diagonal cables give the possibility to create a linear moment along the shaft, where the midpoint of the shaft has a moment of zero.
- A combination of parallel and diagonal cables give a linear moment around the shaft, which can be moved up and downwards.

2.3 Multiple segments

In chapter 2.2 one individual segment is analyzed. However, the maneuverability of one segment is limited. Therefore, it is needed to combine multiple segments.

The segments need to be attached to each other to move as one instrument. This attachment can be done quite straightforward. The top of the first segment can be viewed as the bottom of the second segment. The cables that control the second segment should be led through the first segment. A schematic view of the assumed attachment is presented in Figure 13.

As concluded in Chapter 2.2, it is possible to control the moment at the end of the starting segment. Whenever the second segment is brought in position, this second segment will apply a moment to the first segment at the point of attachment. This moment can be countered, with the cables in the first segment. Therefore, it is possible to view each segment individually and control multiple connected segments. A simple test with the prototype supported this conclusion.

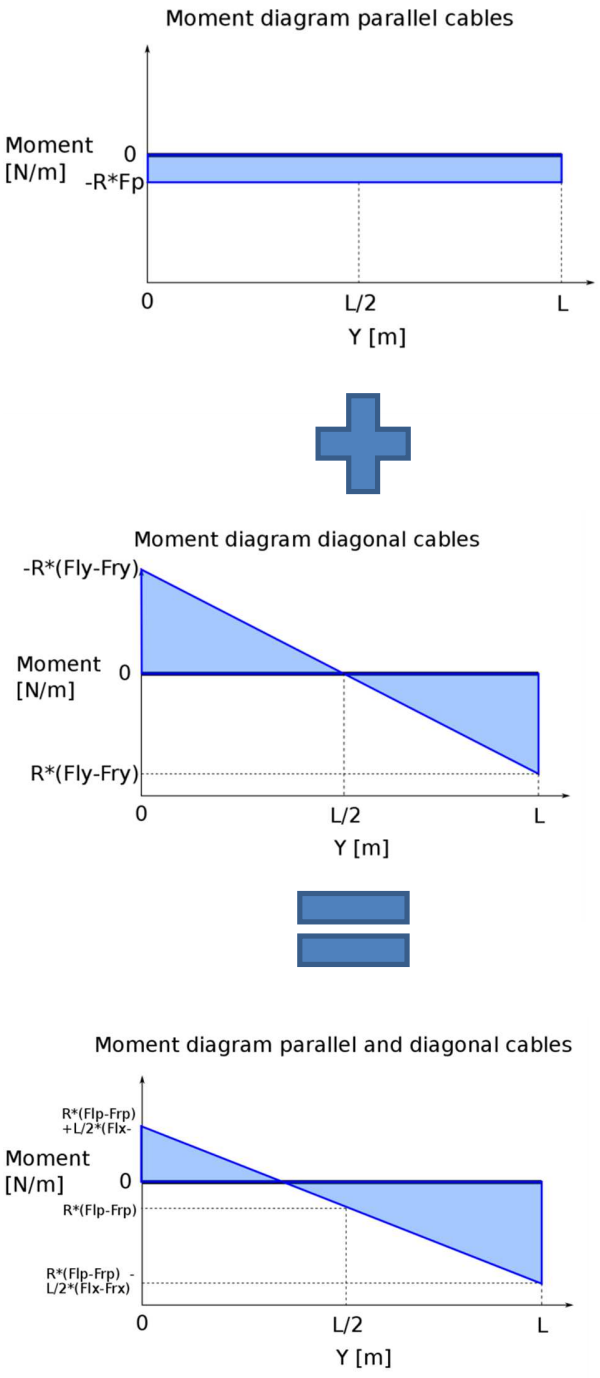

Figure 12: A series of moment diagrams, which added will result in a moment diagram of a segment with parallel and diagonal cables, on all cables is a force applied.

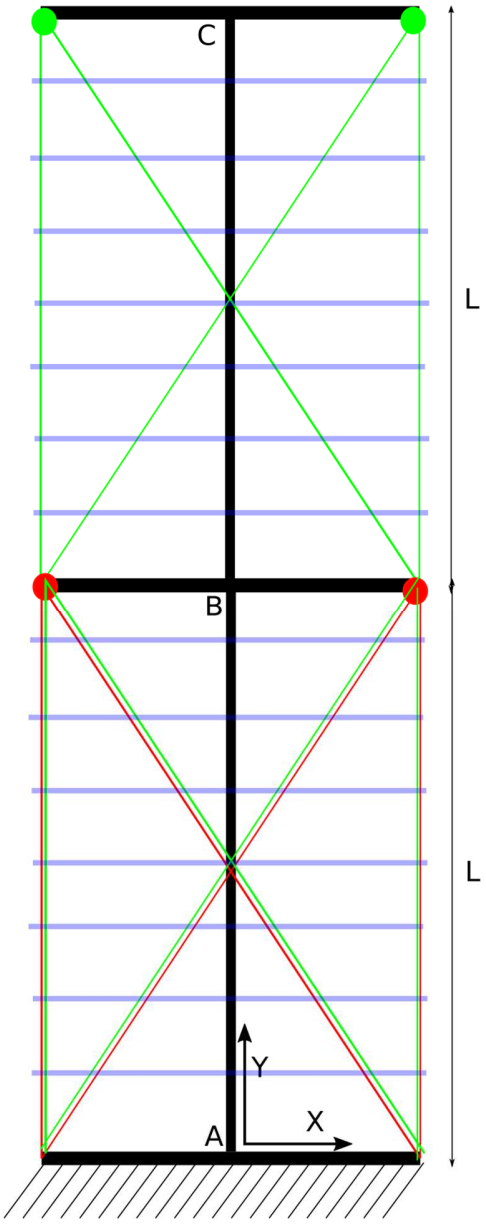

Figure 13: A schematic representation of two segments attached to each other. The orange cables are the parallel cables of the first segment, the red cables are the diagonal cables of the first segment, the blue cables are the parallel cables of the second segment and the green cables are the parallel cables of the second segment. Possible guided ribs are made blue.

2.4 Shape investigation

The different forces all lead to different moment diagrams and therefore, different deformations. These deformations define all possible shapes a segment could form. A combination of shapes of multiple segments would eventually give the working range of the total instrument.

2.4.1 Premises

To calculate the possible shapes of a segment with the help of forces and moment diagrams some assumptions are used.

I. The friction is neglected
II. The stiffness of the cables is neglected
III. The mass of the components is neglected
IV. The model is a kinematic static representation
V. The material is homogeneous
VI. The material behaves in an elastic manner.
VII. Shear stress can be neglect compared to bending stress.
VIII. The moment diagram does not deform due to the deformation of the segment.

These assumptions are explained below. Notice that assumption VIII is discussed separately in section *2.5 non-linearity*.

I. The friction between the cables and the extra ribs used for guidance are being neglected because adding this friction will make the system much more complicated. Besides, the goal of the research is to compare two cable configurations. When friction is neglected in both models, the influence on the comparison will be minimal.

II. The bending stiffness of the cables is neglected. It is assumed that the cable has high axial stiffness, so the strain of the cables can be neglected.

III. The mass of the components is neglected because the mass is relatively small compared to the cable forces.

IV. The model is a kinematic static representation. This means the dynamics of the system is not taken into account.

V. The material used to produce the segments is homogeneous. This means that the material is uniform throughout the whole segment.

VI. The sixth assumption is that the material behaves in an elastic manner. Whenever plastic deformation will take place, the segment will no longer reshape to its original form. Therefore, all of the deformations need to be elastic deformations. A deformation can be viewed as elastic when the stress caused by the deformation is below the yield strength.

VII. The last assumption is that the shear stress can be neglected compared to the bending stress. The length of the beam is assumed to be relatively long in comparison to the height. To verify this assumption a sample calculation is provided.

Sample calculation

The average shear stress is defined in equation 2.16.

$$\tau = F_x/A \qquad (2.16)$$

$$A = h \cdot b \qquad (2.17)$$

Where τ is the average shear stress in Pa. h is the thickness of the beam in the X-axis in m. b is the thickness of the beam in the direction of the Z-axis in m. A is the shear area in m^2. The shear area is assumed to be rectangular. F_x is the total force of the cables in the x-direction, notated as $(F_{lx} - F_{rx})$ in equation 2.15.

The moments that are applied to the beam were earlier mentioned in the equation's 2.11 and 2.15.

In the example R is the length of a rib and is assumed to be 5mm, L is the length of the segment and assumed to be 30mm, h is 0.2mm and b is 5mm. These assumed values in combination with equation 2.17, make it possible to calculate the area at which the shear stress is applied. They also give the possibility to calculate the maximal moment with equation 2.15. If *Y* is equal to zero the moment is maximal, this results in equation 2.18. Notice that F_x is the total force of the cables in the x-direction, notated as $(F_{lx} - F_{rx})$ in equation 2.15.

Notice that the force on the parallel cables, $(F_{lp} - F_{rp})$ in equation 2.15, are assumed to be zero. Because the parallel cables will increase the moment, however, they will not influence the shear stress. It is investigated if the shear stress can always be neglected, so the maximal ratio between the shear stress and the bending stress is calculated.

$$A = 1.0 \cdot 10^{-6}\ m$$

$$Max\ Mtotal = \frac{L}{2} \cdot Fx = 0.015 \cdot F_x \qquad (2.18)$$

For the maximal bending stress, equation 2.19 will be used.

$$\sigma = -My/I \qquad (2.19)$$

Where σ is stress in Pa, *M* is the internal moment in the beam in Nm. I is the beam's moment of inertia computed around the normal axis in m^4 and y is the distance of the computed point to the neutral axis of the beam in m.

The second moment of inertia can be calculated using equation 2.20

$$I = \frac{b \cdot h^3}{12} \qquad (2.20)$$

$$I = 3.3 \cdot 10^{-15}\ m\text{^}4$$

Filling in equation 2.19 gives:

$$\sigma = \frac{-My}{I} = \frac{-0.015 \cdot F_x \cdot 1.0 \cdot 10^{-4}}{3.3 \cdot 10^{-15}} = -450 \cdot 10^6 \cdot F_x \, Pa$$

Filling in equation 2.16 gives:

$$\tau = \frac{F_x}{A} = \frac{F_x}{1.0 \cdot 10^{-6}} = 1.0 \cdot 10^6 \cdot F_x \, Pa$$

The shear stress is approximately 1/450st of the bending stress in the sample calculation, so it can be neglected. This is the case because shear stress will only scale linearly with the thickness of the beam (=h), where the bending moment will scale with a factor 3.

2.4.2 Shape deformation

Based on the premises described in Section 2.4.1 it is possible to calculate the deformation of the individual segments. The first equation that is needed for the calculation of the deformation is the Hooke's law. This law can be applied because it is assumed the material behaves in a linear elastic manner.

$$\varepsilon = \sigma / E \qquad (2.21)$$

Where ε is the dimensionless strain, σ is stress in Pa and E is the material's Elastic modulus in Pa.

The deformation of a beam loaded in bending is calculated, instead of a beam loaded in tension. Therefore the flexure equation is also needed. The flexure equation is equation 2.19

Only the maximal stress which is able to occur is interesting, therefore y will be the distance from the neutral axis up until the boundary of the material. So y is equal to thickness h divided by two.

$$1/\rho = -\sigma/(E \cdot y) \qquad (2.29)$$

This combined equation shows that the curvature is depending on the stress, the Elastic modulus and the thickness of the beam. Equation 2.29 is valid for either small or large radii of curvature [23], where the maximal stress is depending on the elastic limit. This means that a material with a high ratio between the elastic limit and the E-modulus will be able to bend further. To give a frame of reference for the maximal bending angle, a sample calculation is provided below.

Sample calculation

For this calculation it is assumed that the segment is made from Titanium, beta alloy, Ti-12Mo-6Zr-2Fe, form the database of CES Edupack [24]. This material is selected due to its ratio between the elastic limit and the Elastic-modulus. This material has an Elastic modulus of 63.1 GPa, and an elastic limit of 1.15 GPa. For the calculation, the thickness h is assumed to be 0.2 mm, the length of the instrument is 30 mm. And y is equal to the thickness divided by two.

$$y = 0.1 \, mm = (h/2) \qquad (2.30)$$

If these properties are substituted in equation 2.28, it will deliver a radius of curvature of

$$\rho = 5.5 \cdot 10^{-3} \; m$$

This radius of curvature will deliver a maximal bending angle, with a constant curvature of

$$\beta = \frac{L}{\rho \cdot 2\pi} \cdot 360 = 312.5^{\circ}$$

Where β stands for the bending angle in degrees. This suggests that a segment can maximally reach a radius of curvature of 5.5 mm. This will result in an angle of 312.5˚ when the curvature is constant. The sample calculation is only providing a frame of reference.

2.5 Non-Linearity

In section *2.2 Force and moment analysis* the moment diagrams before deformation are calculated. However, a deformation might lead to a different moment diagram. In this section the consequences of larger bends will further be investigated. The non-linear calculations are rather complex and cannot easily be validated by an experiment. Therefore, it is decided to study the validation of the calculations in section *2.2 Force and moment analysis* with previous research.

Cosserat model

Whenever a segment is simulated as a Cosserat Rod model, the deformation of a segment that bends into a plane can be greatly simplified. A Cosserat rod model is a model to describe the behavior of a beam while taking the length of the beam into account for the stiffness calculation. The deformation can be simplified to a moment at the end of the Cosserat Rod. This also goes for large bends. The Cosserat rod theory is proven to be useful and accurate for flexible instruments in multiple papers [25-28].

Bernoulli-Euler beam theory

Webster et al. came to the same conclusion using the Bernoulli-Euler beam theory [25]. The Bernoulli-Euler beam theory describes the deflection characteristics of a beam under load. This theory is based on the linear theory of elasticity. Notice that the Bernoulli-Euler beam theory is, however, normally used for small strains and small rotations. The shaft can be modeled as a beam. As long as the cables pass through a sufficient number of cable guides, a constant moment can be reached with cable control [29]. Gravagne et al. [30] also points out that the Bernoulli-Euler beam mechanics will lead to a constant curvature when a constant moment is applied. For inner-plane motions, it is possible to replace the tendons by a moment, instead of adding cable forces [26].

Constant curvature

A constant moment can be reached with parallel cables whenever a sufficient number of guided ribs are used, as demonstrated by Li and Rahn [29]. The model suggests a ratio of R/N=0.4. where R stands for the length of a rib and N stands for the distance between two guided ribs. With this ratio, the maximal displacement of the tip is equal to 0.6L, where L stands for the length of a segment. The theoretical predictions are validated with experiments.

Next to Li and Rahn, Immega and Antonelli (1995), Cie´slak and Morecki (1999), Hanna and Walker (2003) and Jones and Walker (2006) also made a backbone based flexible instrument with three cables [29,31-34]. These models all used guided ribs and they all show a constant curvature. Besides, Webster et al. Claims to research multiple flexible instruments for which a constant curvature approach is applicable [25].

Linear curvature

A model of a 2D instrument with diagonal cables and cable guides is presented by Henselmans [35]. This model divides one segment into multiple sub-segments between each conductive rib. The model assumes that each section of the flexible shaft between two cable guides can only bend with a constant curvature. On the basis of this assumption, the moment of each sub-segment is calculated. This results in a deformation for each sub-segment. A combination of those deformations will result in the shape of the total segment. The model of Henselmans shows a linear curvature with corners up to 90 degrees. Larger deformations could also be calculated, however, the report lists that this will result in non-linear behavior

[35]. The results of the model of Henselmans are validated with a physical prototype of the model.

Assumption

A bent segment will result in a deformed shaft. Whenever the cables are attached to the top ribs and do not pass through enough cable guides, the deformed shaft will adjust the direction of the cables. The change in direction will influence the moment and therefore the moment diagram. However, if the cables pass through a sufficient number of cable guides, this effect is limited [29].

On the basis of the previous research, it has been decided to assume a constant curvature for the segment with the parallel cables, and a linear curvature for the segment with the parallel and diagonal cables. This assumption makes the calculations usable for other flexible instruments with a linear or constant curvature.

2.6 Possible shapes

The different configurations lead to different moment diagrams. These different moment diagrams lead to different curvatures. Equation 2.19 and 2.29 can be combined to form equation 2.31. This equation shows that the bending moment is inversely proportional to ρ and therefore proportional to the curvature.

$$1/\rho = M/(E \cdot I) \qquad (2.31)$$

This conclusion leads to the shape possibilities of different configurations. A configuration with two parallel cables is capable of delivering a constant bending moment, see Section 2.2.1. A constant bending moment will result in a constant curvature. This means that the possible shapes are defined as a part of a circle. The radius of the circle is variable. This means that the end angle of the segment is dependent on the end location of the segment. Figure 14 gives an impression of possible shapes.

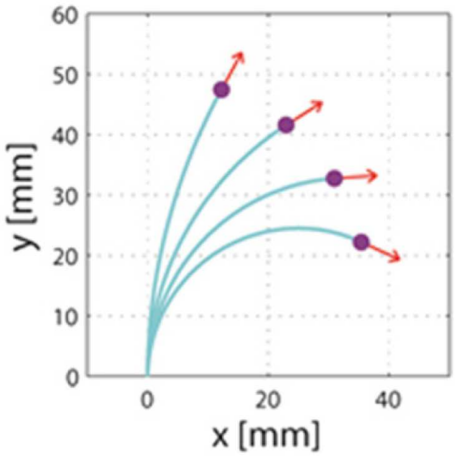

Figure 14: A schematic overview of possible shapes made by a segment with two parallel cables [14].

A configuration with two diagonal cables is capable of delivering a linear bending moment which is zero at the center of the shaft, see Section 2.2.2. A linear bending moment will result in a linear curvature. The shape will, however, always be symmetrical from the center of the shaft. This means that the end angle of the segment is always the same as the start angle of the segment. Figure 15 gives an impression of possible shapes.

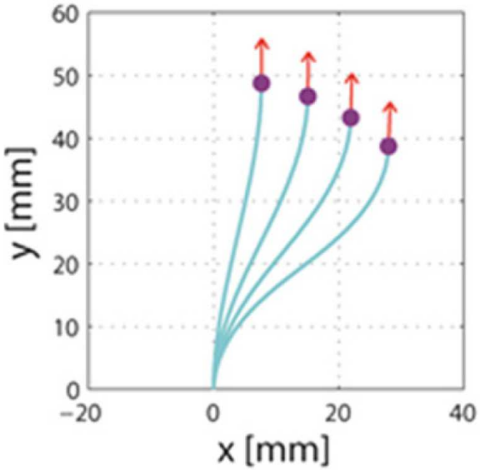

Figure 15: A schematic overview of possible shapes made by a segment with two diagonal cables [14].

A configuration with two parallel and two diagonal cables is capable of delivering a linear bending moment, see Section 2.2.3. A linear bending moment will result in linear curvature. The other configuration shows parallel and diagonal cables.

The shape does not need to be symmetrical from the center of the shaft, in contradiction to the configuration with only diagonal cables. This means that the end angle of the segment is independent of the end location of the segment. See Figure 16.

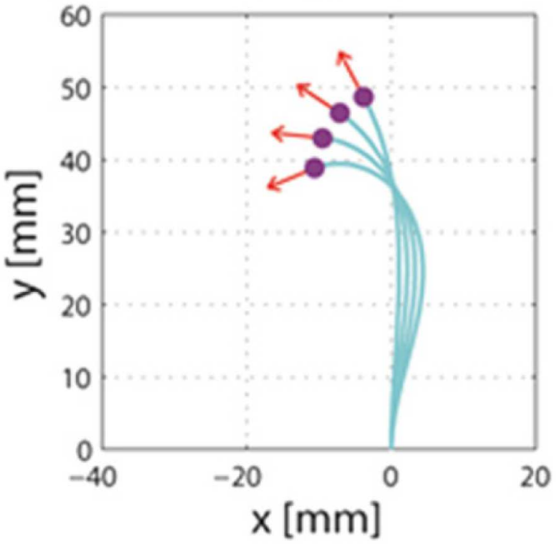

Figure 16: A schematic overview of possible shapes made by a segment with two parallel and two diagonal cables [14].

The overview of the three different configurations teach us the kinematic differences.

- Parallel cables give the possibility to create a constant curvature and therefore circle-like shapes.
- Diagonal cables give us the possibility to create a linear curvature and therefore s-like shapes, however, the end angle will always be equal to the start angle.
- A combination of parallel and diagonal cables give us a linear curvature, with the same possibilities of the previous configurations. However, in this case, the end angle is independent of the end position.

3. Kinematic simulation of multiple segments

Intro

In this chapter, the calculations involving the workspace of the instrument are described. The calculations are done with MATLAB R2015a. The calculation method will also be discussed for one and multiple segments. Together with the integration in the MATLAB code.

The MATLAB code is written to get an insight of the possible configurations an instrument with multiple segments can achieve. This is done by defining an optimal path. The results will be used to compare the performance of the two different configurations.

The kinematic simulation uses the constant curvature and linear curvature shapes found in chapter 2. It was decided to base the simulation on possible shapes instead of a cable length or force calculation to generate general results that are also applicable on future instruments if other types of manufacturing are used.

3.1 Path optimizing

For the selection of the most promising cable configuration, a mechanical system is translated into an algorithm. This specific algorithm is capable of predicting the maneuverability of the instruments.

Transmitted information

As mentioned earlier, the control of the instrument will be done with the aid of a preformed shaft. An example of a schematic representation of the preformed shaft can be seen in Figure 17. The master and the slave exist of the same type of segments. Thus, the master for the simple slave only has parallel cables, and the master for the complex slave has parallel and diagonal cables. The master will follow the preformed shaft and will transmit the shape of the shaft to the slave, via cables. The master is, however, not able to transmit the whole shape. It is only capable of transmitting one angle or one angle and one position per segment, depending on the cable configuration. This means that the master and the slave can have different shapes, as long as the end angle and the end position of the segments are equal. The information that the master is transmitting to the slave is the red dots in Figure 18. These red dots can contain the desired end angle of a segment, and in case of the parallel and diagonal cables also the desired end position of a segment.

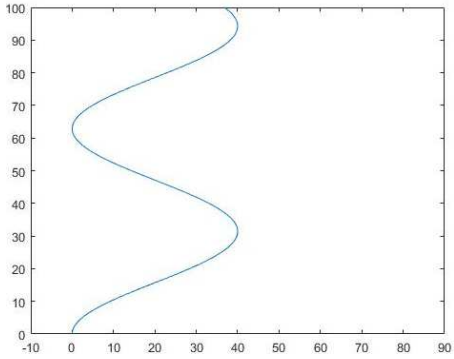

Figure 17: A schematic representation of the desired path.

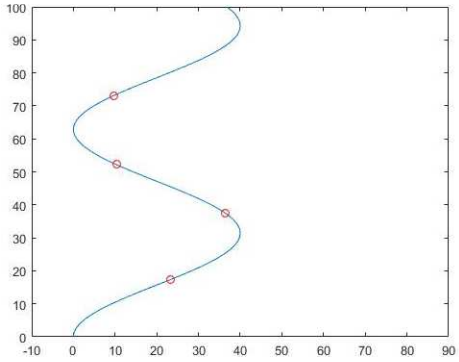

Figure 18: A schematic representation of the desired path together with the desired points.

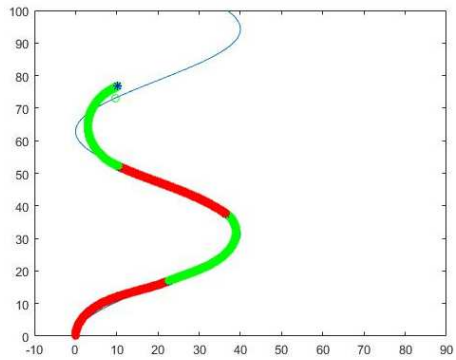

Figure 19: A schematic representation of a calculated slave.

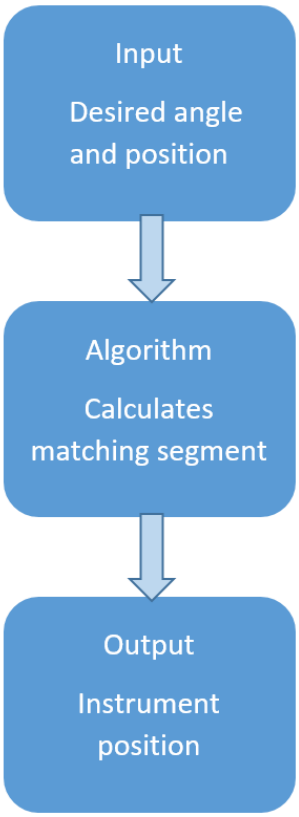

Figure 20: A schematic view of the code

The used algorithm first determines the positions, which will be reached if the segment completely overlaps the ideal path. Each of these positions has an end angle, which is the desired angle on this point.

Simple segment information

Simple segments with a constant curvature only have one DOF, hence it is possible to optimize to a certain position or towards a certain angle. The combination of both is, however, impossible. The mechanical system that is modelled will be able to transmit only an angle from the master to the slave. So the segments in the algorithm will be optimized towards the transmitted angle.

For the simple configuration, the red dots presented in Figure 18 will only deliver an end angle of every segment. So each red dot stands for an angle at the position on the path. This is all the information delivered to the simple slave.

Complex segment information

Segments with a linear curvature, have two DOF, this makes it possible to calculate the shapes with the precise end angle, and select the best matching position. This will increase the probability of the best matching segment with the ideal path.

For the complex configuration, each red dot represented in Figure 18 stands for a position and an angle at that position. This is all the provided information to the complex slave.

Information use

The end angle and end position are used as input properties for the MATLAB algorithm. The MATLAB algorithm calculates the slave, see Figure 19. The MATLAB algorithm will eventually calculate the difference between the path that is followed by the master, and the path that is formed by the slave.

A schematic overview of the code can be seen in Figure 20. Firstly the desired angles (and positions) are calculated. These properties are loaded into the algorithm. The algorithm

calculates the form of the slave. The end position of the slave is the output of the algorithm.

3.2 Shape determination

In chapter 2 a connection between the moment diagram and the curvature is made. In this section, this connection is worked out to the possible shapes a segment can develop. The kinematics of the different configurations can be divided into segments with a constant curvature and segments with a linear curvature.

Constant curvature

The segment with a constant curvature can be described with as a part of a circle bow. If the total angle is given the radius of the circle can be determined by the following equation:

$$r = \frac{L}{\alpha} \tag{3.1}$$

Where r stands for the radius of curvature in m, L stands for the length of one segment in m and α stands for the angle of a segment in rad. Together with the radius and the angle, the x and y position can be determined.

$$x = r(1 - \cos(\alpha)) \tag{3.2}$$

$$y = r\sin(\alpha) \tag{3.3}$$

Linear curvature

Segments with a linear curvature can be described with an Euler spiral. An Euler spiral also known as clothoid or Cornu spiral, is a curve whose curvature linearly increases or decreases with its curve length. As can be seen in Figure 21, the radius of curvature is largest in the middle of the figure. When moving to the sides the radius of curvature decreases. This radius of curvature decreases linearly to the traveled distance from the center.

An Euler spiral can be described with the Fresnel integral, which gives the following equations:

$$X(t) = \int_0^t \sin(u^2)\, du \tag{3.4}$$

$$Y(t) = \int_0^t \cos(u^2)\, du \tag{3.5}$$

Where t is the arclength from the orgin to the point $(X(t), Y(t))$ and u is the total arc length of the spiral.

Because the Euler spiral is a function with a linear curvature, every function with a linear curvature can be described as a part of the Euler spiral.

The starting point on the Euler spiral defines the begin curvature of the segment. This starting point is also connected with a radius of curvature and therefore with a curvature.

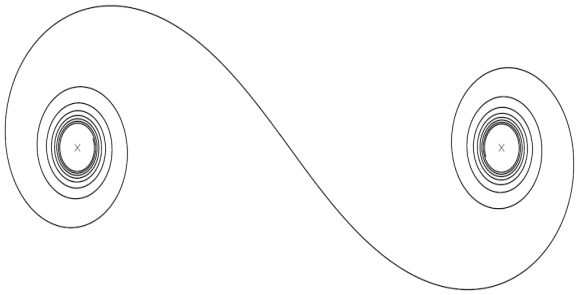

Figure 21: Euler spiral [36].

The scaling factor in combination with the starting point, define the endpoint on the Euler spiral. Because the length of the segment is predefined, the scaling factor determines the relative distance from the starting point to the end point on the line. The ends point is also coupled to a curvature.

Whenever the begin- and end-curvatures are known, the curvature of all the points between the starting point and endpoint, so all the points of the segment, are also known. The curvature of these points increases or decreases linear with the distance.

If the segment length is constant the starting curvature and the slope of the curvature decide the end curvature. Because the starting curvature and the slope of the curvature can be adjusted, every possible line with a linear curvature can be found on a scaled Euler spiral.

Multiple segments

Multiple segments need to be attached to each other. The end point of one segment is the starting point of the next segment. Notice that next to the position the direction is also forwarded to the next segment.

3.3 Calculation structure

Intro

This section will describe the structure of the calculation. The first step in the calculation is the definition of the desired path. The desired points and angles will be determined. The second section describes the global and local frames. Next, the segment calculation will be discussed. Afterwards, the error calculation and the validation will be explained.

3.3.1 Desired path for the simple and complex segments

The instruments need to optimize towards a certain path. This path is defined by the performed shaft. In the code, the path can be defined and manipulated in the script code. The x and y-coordinate of the path are described separately with one variable called t, and can be defined by a number of mathematical expressions. x and y are independent.

Determine desired points

The desired points are the points on the path to which the segments optimize. The first desired point lays one segment length from the starting point traveled along the desired path. The second desired point is again a segment length further from the first desired point.

To determine the position of the desired points, the length of the path should be calculated. This is done with the Euler method. First, the derivative of the x and y curves is taken with respect to the independent variable called t, done with the help of the symbolic toolbox of MATLAB. After taking the derivative of the functions x-curve and y-curve, the step-size is defined. This step-size is directly related to the accuracy of the calculation. The arc-length is defined by the length of the instrument. After traveling the arc-length over the desired path the x and y position is saved as the desired point.

Determine angle of desired points

To determine the desired angle, the derivative of the desired path is needed. The path is divided into a large number of points. The derivative of the path can be used to calculate the direction of every point on the path.

A clockwise angle is defined positive, and the y line is defined as an angle of zero radians. This calculation needs, however, two exceptions.

First of all, the calculation will deliver the same angle, when both derivatives are positive as when both derivatives are negative, while the angle is certainly different. This is solved by adding the following exception, when both of the derivatives are negative, π is added to the found angle, to define an angle in the opposite direction.

When one of the derivatives is negative, so a negative dx or a negative dy, the angle will be calculated, however, the direction will be opposite. If dy is negative but dx is positive, π is added to the angle, when dx is negative but dy is positive, the normal angle will be calculated.

3.3.2 Global and local frames

All the calculations are done in multiple frames: a global frame, which is the same for all the segments, and multiple local frames. Each of the segments has a local segment frame, and each of the segments is firstly calculated in the Euler spiral frame.

Notice that the simple segments of the constant curvature do have a global frame and a local segment frame. However, they do not have an Euler spiral frame.

Simple segment frames

The simple segments have a global frame, wherein the desired path is defined. All the calculated segments are eventually exported to this global frame. Thus the global frame will represent the shape of the total instrument, after calculation.

The information of the desired end angles and the endpoints are translated from the desired path to the local frame. In this local frame, the segment will be calculated. This segment is afterward exported to the global frame. For a representation of the local frames in the global frame see Figure 22.

Global frame of the complex segment

The global frame is the frame where all the desired points and the respective desired angles on the desired path are calculated. Besides the desired points, the final instrument segment solutions are also converted to the global frame. In Figure 22 the global frame is shown, with the local segments frame in it.

The local segment frame of the complex segment

The desired points and angles are converted to the local segment frame. Figure 22 gives an overview of multiple local segments frames plotted in the global frame. The local frames are a translation and rotation compared to the global frame. The rotation is done with an Euler rotation matrix.

The desired points are described in the global frame. These desired points are translated and rotated to be described into the local segment frame. The use of a local frame makes it possible to use the same calculation method for every segment.

The possible shapes of the segments are calculated in the Euler spiral frame and transferred again to the local segment frame. The selection of the segment is done in the local segment frame.

The selected segment is in its turn again transferred to the global frame. This is done with a rotation matrix together with a translation.

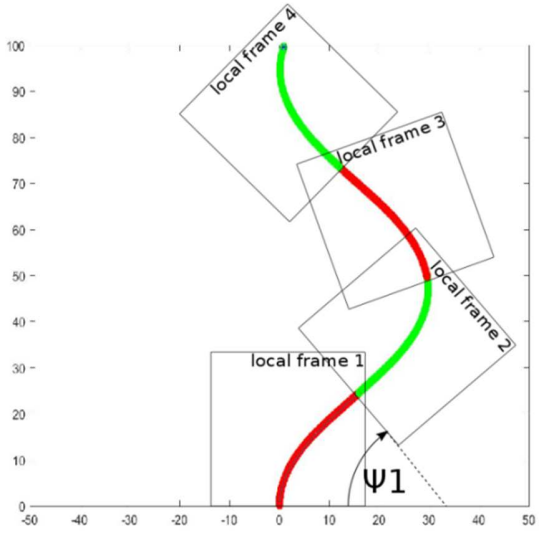

Figure 22: Local frames in the global frame.

The local Euler spiral frame of the complex segment

The Euler spiral frame is represented in Figure 23. On the Euler spiral, different starting points are selected. Whenever a part of the Euler spiral is selected as a shape for the instrument, this part needs to start in an upwards direction.

Otherwise, it is not possible to paste this segment on top of the previous segment. See Figure 24 for an example.

All these starting points have an angle compared to a reference point. The reference point is the center point of the Euler spiral. Each possible segment on the Euler spiral needs to be rotated, with the angle belonging to the starting point in order to translate the Euler frame to the local frame.

As can be seen in Figure 24, the Euler spiral is rotated so that the instrument starts at a vertical position. The segment is the thick red line consisting of circles, while the whole Euler spiral is a thin red line. To convert the Euler spiral in Figure 23 to a local Euler spiral of Figure 24 it has to be rotated with the angle of the starting point. The local Euler spiral is different for each point on the Euler spiral.

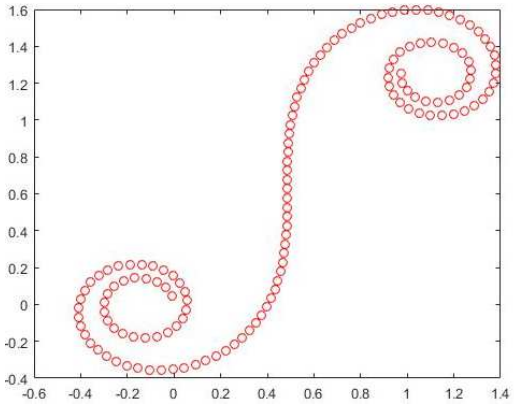

Figure 23: Euler spiral frame.

Overview of the complex segment frames

Thus the segments are calculated on the Euler spiral frame. The segments in the Euler spiral frame are rotated to the local segment frame. The information of the desired path in the global frame is rotated to the local segment frame. The segments of the Euler spiral are selected in the local segment frame. Finally, the selected segment in the local segment frame is rotated and translated to the global frame.

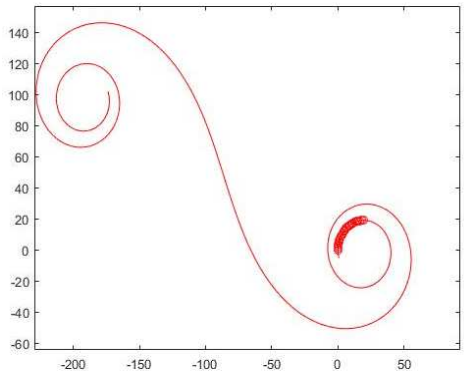

Figure 24: Rotated Euler spiral.

3.3.3 Simple segment calculation

The segment calculation can be divided into three steps

- Endpoint calculation
- Shape calculation
- Segment rotation

Endpoint calculation

Firstly the desired angle will be translated to the possible shape of the segment. For the calculation of the x and y coordinates at the end of the segment, the Equation's 3.1-3.3 are used. For these equations the absolute value of the angle will be used. If the desired angle is negative, the x coordinate is multiplied by minus one, and therefore rotated in the other direction.

Notice that the calculation of Equation 3.1 is not possible if the angle approaches zero. Whenever the angle is smaller than 0.001 radians, y assumed to be equal to the segment length and x is assumed to be zero.

Shape calculation

The second step is to calculate a defined number of points between the start point of the segment and the endpoint of the segment.

These points lay on the shape of the segment and are used for the performance check at the end of the code.

Segment rotation

For this rotation of the segment from the local to the global frame an Euler rotation matrix is used, see equation 3.6. Whenever the x- and y-coordinates in the local segment frame will be rotated with the Euler matrix, the x- and y-coordinates in the global frame can be calculated as shown in Equation 3.7.

$$\mathrm{R}(\theta_1) = \begin{bmatrix} \cos(\theta_1) & -\sin(\theta_1) \\ \sin(\theta_1) & \cos(\theta_1) \end{bmatrix} \quad (3.6)$$

$$\begin{bmatrix} X_l & Y_l \end{bmatrix} = \begin{bmatrix} \cos(\theta_1) & -\sin(\theta_1) \\ \sin(\theta_1) & \cos(\theta_1) \end{bmatrix} \begin{bmatrix} X_s \\ Y_s \end{bmatrix} \quad (3.7)$$

Translation

Besides the rotation, the segment also needs to be translated. The starting point of the current segment should match the end point of the previous segment. This is done by firstly translating the starting point of the current segment to the origin. The x- and y -coordinates of the end position of the previous segment, will afterward be added to the coordinates of the current segment. This will result in two connecting segments.

3.3.4 Complex segment calculation

The segment calculation can be divided into five steps.

- Selecting the starting points
- Calculating the matching endpoints
- Scaling the segment
- Rotating and translating the segment
- Selecting the best match

Selecting the starting points means starting with a number of starting points on the Euler spiral. The matching endpoints that make the desired angle relative to the starting points are calculated. These endpoints lay on the Euler spiral as well. The path from the starting point over the Euler spiral to the endpoint will give the shape of the segment. This segment needs to be scaled, which will be explained in *scaling the segment*. Afterwards, these shapes are rotated to the local frame, to be compared to the desired endpoint. Finally, the selection of the best fitting segment takes place. These processes are further described in this section.

Selecting the starting points

The complex instrument segment calculation and selection starts with a number of starting points. These starting points are points on the Euler spiral. The number of starting points is defined by the length of the Euler spiral and the step size between every starting point. A higher number of starting points results in a higher number of calculated segments. Whenever the step-size is reduced, it will increase the precision. Both the step-size and the length of the Euler spiral are defined in the script file.

Figure 23 shows a number of starting points on the Euler spiral, every red circle stands for a starting point. The number of starting points generated in Figure 23 is relatively low to give a clear image. Each starting point on the Euler spiral has one or more matching endpoints.

To determine the possible endpoints for each starting point, the angle of the starting point is defined relative to the center of the Euler spiral, see equation 3.8. This equation is a definition of the Euler spiral.

$$\alpha \sim dl^2 \quad (3.8)$$

$$\alpha = \text{the starting angle in rad}$$

$$dl = distance\ to\ the\ center\ in\ mm$$

The Euler spiral has a linear curvature. This means that the angle scales with a power of two compared to the distance from the center.

Because all the starting points are all numbered, the first starting point gets the number one the second one gets the number two and so on, the equation in the code is equation 3.9.

$$\alpha = \left(i - 0.5 \cdot (Ns + 1)\right) \cdot h \qquad (3.9)$$

Where

$$\alpha = \ starting\ angle\ in\ rad$$

$$i = the\ number\ of\ the\ starting\ point$$

$$h = the\ stepsize\ between\ starting\ points$$

$$Ns = the\ total\ number\ of\ steps$$

This angle stands for the rotation of the local Euler spiral frame, which is needed to rotate the shape to the local segment frame.

Calculating the matching endpoints

Each of the starting points has at least one matching endpoint. This endpoint has a relative angle to the center of the Euler spiral, same as the starting point.

The difference between the angle of the starting point and the end point is called the relative angle. This angle should be equal to the desired angle, the angle that the segment should create.

$$end\ angle - starting\ angle = relative\ angle \qquad (3.10)$$

$$relative\ angle = desired\ angle \qquad (3.11)$$

However, there are multiple points that have a relative angle to the starting point that is equal to the desired angle.

These angles will be converted into positions on the Euler spiral. The Equation 3.12 gives the position before the center of the Euler spiral, the Equation 3.13 gives the position past the center of the Euler spiral.

$$Ni = \frac{\sqrt{\beta}}{h} + \frac{Ns-1}{2} \qquad (3.12)$$

$$Ni = -\frac{\sqrt{\beta}}{h} + \frac{Ns-1}{2} \qquad (3.13)$$

$$\beta = desired\ angle\ in\ rad$$

$$Ni = the\ number\ of\ the\ endpoint$$

$$h = the\ stepsize\ between\ starting\ points$$

$$Ns = the\ total\ number\ of\ steps$$

The number of the endpoint is a number that is coupled to a location on the Euler spiral. The same goes for the number of the starting point. However, the number of the endpoint is not an integer. The number stands for the number of step-sizes traveled over the Euler spiral curve.

If the angle is in the other direction, the Euler spiral will be mirrored to calculate the matching end points. The information of a start and an endpoint, gives the possible shapes of the instrument.

Scaling the segment

Whenever the starting points and the matching end points are selected, it is time to scale the segments to the appropriate size.

The segments are scaled with a scaling factor. To calculate the scaling factor two things should be known, the length of the unscaled segment, and the final length of the segment.

The length of the unscaled segment can be calculated with the following equation.

$$abs(i - Ni) \cdot h = L_0 \qquad (3.14)$$

Where

$$L_0 = unscaled\ length\ in\ mm$$

$$i = the\ number\ of\ the\ starting\ point$$

$$Ni = the\ number\ of\ the\ endpoint$$

$$h = the\ stepsize\ between\ starting\ points$$

The final length of the segment is predefined in the properties of the code.

The scaling factor can be calculated with the following equation.

$$SC = \frac{L_f}{L_0} \tag{3.15}$$

Where

$$L_f = final\ length\ in\ mm$$

$$L_0 = unscaled\ length\ in\ mm$$

$$SC = scaling\ factor$$

The needed scaling factor is determined for every start-point with each possible end point, in this case, two per start point.

The start and end point number indicate the position on the Euler spiral and can be subtracted. Whenever the difference is multiplied by the step-size, the unscaled segment length is calculated. This unscaled segment length should be multiplied by the scaling factor to reach the final segment length.

Calculating the x and y coordinates

The x and y coordinates can easily be calculated. This is done with the aid of the Fresnel's integral. See equation 3.4 and 3.5.

Rotating and translating the segment

The next step is to convert the x and y-coordinates in the Euler spiral frame to coordinates in the local segment frame. This needs to be done because the desired endpoints are expressed into the local segment frame.

For this rotation, an Euler rotation matrix is used, see equation 3.6. Whenever the x and y-coordinates in the segment frame will be rotated with the Euler matrix, the x and y of the local frame can be calculated, as shown in equation 3.7. The same principle is used to rotate the segment in the local frame to the global frame.

Translation

Besides the rotation, the segment also needs to be translated. The starting point of the current segment should match the origin of the local segment frame.

Selecting the best match

All the different endpoints of the segments can be described in x and y-coordinates. All these x and y-coordinates are stored in a vector. This will give the possibility to compare the x and y – coordinates with the desired end location of the segment. The root mean square error is taken, and the segment with the smallest error will be selected. Notice that this calculation takes place in the local segment frame, so afterward the segments are translated to the global frame.

Recalculation

The selected segment will be calculated again, but this time not only with a starting point and an endpoint, but also with a defined number of points in between. This is done for the performance check at the end of the code.

Afterwards, the segment is rotated and translated to the global frame. This happens in the same manner as the rotation and translation of the simple segment.

3.3.5 Error calculation

To measure the performance of a segment, it is possible to value the error compared to the desired path.

It can be noticed that the preselection of the best segment is not decided on the error compared to the desired path, but instead to the error of the endpoint. It is not possible to physically control the total curve of the segment, therefore the selection is based on the endpoint.

There are multiple methods to define the error of the instrument compared to the ideal path.

Because all the different error methods have pros and cons, multiple common error methods will be discussed in this section.

Error

To calculate the error of the instrument in comparison with the desired path, it is decided to compare the calculated points of the instrument, with defined points on the desired path. These are the defined number of points on the instrument are equally divided along the instrument with a total of 4000 points. The path is also defined in multiple points. The points on the path lay 1 µm from each other. Assuming the path approaches a straight line between the two points, the maximal error that can occur due to error measurement is 0.5 µm. This measurement error can be neglected, compared to the error formed by the instrument following the path. The calculated points of the instrument are individually compared to a number of points distributed along the desired path. This is done with the help of a double loop function.

Firstly, an x-coordinate and a y-coordinate of a point on the instrument is taken. The first x-position and y-position on the desired path are subtracted from the x-position and a y-position of the instrument. This subtraction gives a difference in x and y. This difference is squared and added up. Afterwards, the root of this result is taken. This error is saved in a vector. The next step is to compare the first selected x and y coordinates of the instrument with the next x and y coordinates of the desired path. When the first point of the instrument is compared to all the points on the desired path, the minimal error is selected. This calculation will take place for all different x and y coordinates of the instrument.

Root mean square error

To calculate the root mean square error the root square error is needed. The root square error is already calculated in the previous step, these root square errors are all added up and divided by the number of errors to determine the root mean square errors.

Standard deviation

The standard deviation of the error is calculated to give extra information to the root mean square error.

Square error

A square error plot is made by taking the square of every individual error, the reason for this plot is due to the larger errors are assumed to be exponentially more damaging compared to the smaller errors. So the sum of all the squared errors might be a better measurement.

Number of large errors

The number of large errors is a way of determining the number of errors which are relatively larger. This boundary can be set at for instance 3 mm, to filter out the smaller errors. The smaller errors are less important and will therefore not be shown by this way of measuring. To measure the number of larger errors, all the errors are compared to the boundary of 3 mm. The total number of errors higher than 3mm is shown in a percentage of the total number of measured errors.

Maximal and minimal error

The maximum error is an important value to put the other root mean square errors in perspective. The minimum error is also calculated , however, this will always result in an error of zero if the starting point of the instrument lays on the desired path.

Rounded error

All individual error components are rounded to the closest integer. This will show a clear division in the size of errors.

Median error

The median error is determined. The median is less influenced by strong outliers, but outliers

are important in this error calculation so the median error is less important.

Histogram

A histogram gives a clear overview of how much an error of a size range occurs. This method gives a fast broad overview of the errors.

3.3.6 Validation

To control the algorithm different ways of validation are introduced. Many of these ways of validation are based on the knowledge of the observer.

The first way of validation is the end angle control. Whenever the end angle of the segment is not equal to the desired end angle in the global frame, the algorithm will show an error. This code makes sure the end angle of the segment and the desired angle are equal.

The second way of validation is the end error control. The end angle is recalculated in the script file. Whenever this end error is not equal to the calculated end error, the algorithm will display an error.

The third way of validation is the segment plot. Each segment is plot as a part of the Euler spiral. This plot can be compared to the final segment plot to check if the segment is indeed possible to make.

The fourth way of validation is the end plot. Although this plot is more complex to verify, the results can be compared to the expected outcome.

4. Case studies

Intro

The two different configurations can be compared by choosing multiple shapes that the instruments should be able to form. Because this is a static and not a dynamic study it is decided to map the segments over different paths, instead of moving segments over different paths.

To compare the performance of different configurations seven paths have been designed. These paths are mathematical paths to decide the maneuverability of the segments. The decision to perform mathematical paths instead of medical paths is made to increase the objectivity, medical paths are more difficult to categorize and even more arbitrary to select.

The mathematical cases that will be used for reference are a straight line, two exponential equations, two sinusoids, and two equations consisting of combined circular arcs.

The straight line is selected to validate the algorithm. Besides, it will give an impression of the accuracy of the algorithm.

The exponential equations are selected because they are an example of a relatively sharp curve with a small radius. Therefore, both paths are important to show the ability in follow bends of the instruments.

The sinusoids are selected to compare the instruments on their ability to form a complex shape, with multiple corners. The sinusoid will have a relatively high frequency to force the different instruments to form multiple curves.

The paths consisting of two combined circular arcs are introduced to measure the capability of an instrument with constant curvature segments to follow a path with two different constant curvatures.

Names

- Case 1 straight
- Case 2 exponential
- Case 3 sinusoid
- Case 4 circular arcs

The instrument is chosen to be 120mm long.

4.1 Case 1 straight

The first path is a straight line. This path is used to validate the algorithm. Besides, the path gives us insight into the accuracy of the error calculation.

The shape of this path is written down in the equations 4.1 and 4.2.

$$X = 0 \tag{4.1}$$

$$Y = t \tag{4.2}$$

The equations used in the code are 4.3 and 4.4.

$$X = 1 \cdot 10^{-11} \cdot t \cdot t^{10^{-11}} \tag{4.3}$$

$$Y = 30 \cdot t \cdot t^{10^{-11}} \tag{4.4}$$

The equation is noted differently in the code because the code needs a second derivative that is not equal to zero, for the calculation of the direction of the path. Notice that the equation used in the algorithm is an accurate approximation of the original equation. The path is presented in Figure 25.

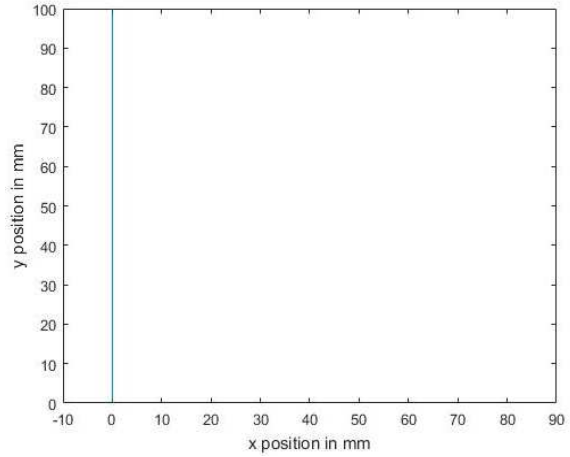

Figure 25: A schematic representation of path case 1

4.2 Case 2 exponential

The second shape is an exponential equation. This basic mathematical equation is able to show the capability of an instrument in forming a path with a sharp curve followed by a straight line. This shape is presented in two forms to increase the reliability of the results. The first exponential equation can be described with the equations 4.5 and 4.6.

$$X = 5 \cdot t^2 \quad (4.5)$$

$$Y = 20 \cdot t \quad (4.6)$$

The equations used in the code are 4.7 and 4.8.

$$X = 5 \cdot t^2 \quad (4.7)$$

$$Y = 20 \cdot t \cdot t^{10^{-11}} \quad (4.8)$$

The path is presented in Figure 26.

The second exponential form can be described with the equations 4.9 and 4.10.

$$X = 5 \cdot t^5 \quad (4.9)$$

$$Y = 20 \cdot t \quad (4.10)$$

Notice that the higher power in equation 4.9 will result in a sharper curve and the path is, therefore, harder to follow. The equations used in the code are 4.11 and 4.12.

$$X = 5 \cdot t^5 \quad (4.11)$$

$$Y = 20 \cdot t \cdot t^{10^{-11}} \quad (4.12)$$

The path is presented in Figure 27.

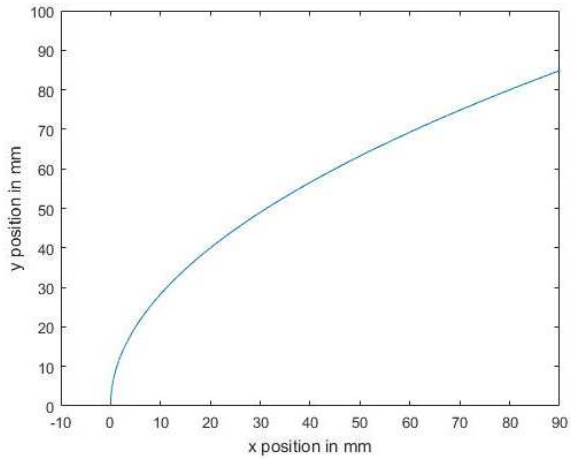

Figure 26: A schematic representation of path case 2 version 1

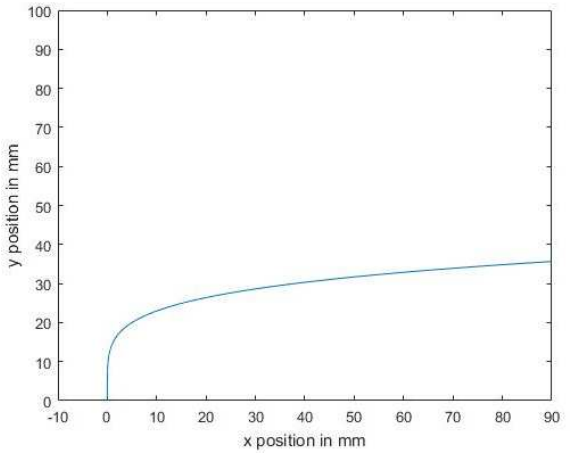

Figure 27: A schematic representation of path case 2 version 2

4.3 Case 3 sinusoid

The third shape is a sinusoid. A sinusoid is a continuous mathematical equation, with multiple changes in direction, and therefore an

interesting path. The radius of curvature constantly chances among the path, which makes the form difficult to follow. To improve the reliability of the results it is decided to define two sinusoid paths. The first sinusoid can be described with the equations 4.13 and 4.14.

$$X = -30 \cdot \cos(t) + 30 \quad (4.13)$$

$$Y = 20 \cdot t \quad (4.14)$$

The equations used in the code are 4.15 and 4.16.

$$X = -30 \cdot \cos(t) + 30 \quad (4.15)$$

$$Y = 20 \cdot t \cdot t^{10^{-11}} \quad (4.16)$$

The path is presented in Figure 28.

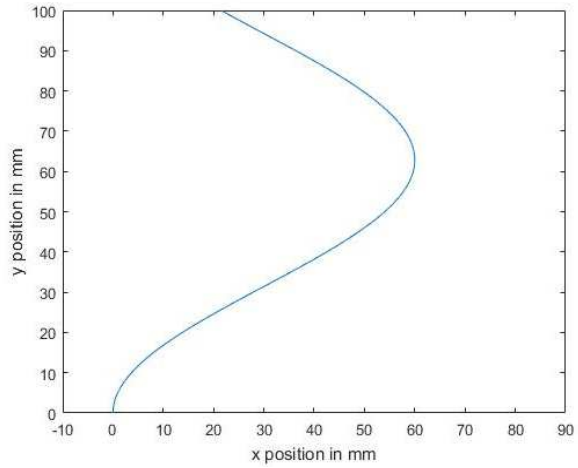

Figure 28: A schematic representation of path case 3 version 1

The second sinusoid has more and sharper angles and can be described with the equations 4.17 and 4.18.

$$X = -20 \cdot \cos(t) + 20 \quad (4.17)$$

$$Y = 10 \cdot t \quad (4.18)$$

The equations used in the code are 4.19 and 4.20

$$X = -20 \cdot \cos(t) + 20 \quad (4.19)$$

$$Y = 10 \cdot t \cdot t^{10^{-11}} \quad (4.20)$$

The path is presented in Figure 29.

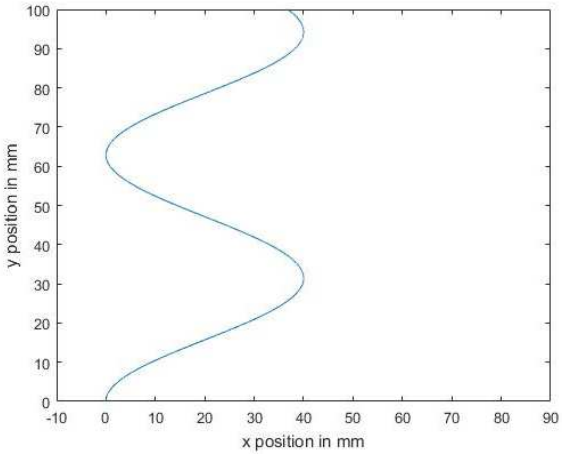

Figure 29: A schematic representation of path case 3 version 2

4.4 Case 4 circular arcs

The fourth shape is two circular arcs added to each other. This shape is a continuous equation, with two constant curvature arcs. Either instrument should be able to form a constant curvature arc. However, a path that consist of multiple parts with different constant curvatures is probably more difficult to follow.

To improve the reliability of the results, it is decided to define two paths with multiple circular arcs. Two mathematical equations are designed based on this concept. The first form can be described with the equations 4.21 and 4.22.

$$X = (40 \cdot \cos(t) - 40) * H\left(\frac{1}{3}\pi - t\right) + \left(-40 \cdot \cos\left(\frac{2}{3}\pi - t\right)\right) \cdot H\left(t - \frac{1}{3}\pi\right) \quad (4.21)$$

$$Y = 40 \cdot \sin(t) \cdot H\left(\frac{1}{3}\pi - t\right) + (80 \cdot \sin\left(\frac{1}{3}\pi\right) - 40 \cdot \sin(\frac{2}{3}\pi - t)) \cdot H\left(t - \frac{1}{3}\pi\right) \quad (4.22)$$

The H in this equation stands for a Heaviside function. This equation results in a circle bow with an angle of 1/3 π. After this circle bow, the path continues with another circle bow with the same radius but an opposite direction.

The equations used in the code are 4.23 and 4.24.

$$X = (40 \cdot \cos(t) - 40) \cdot Heaviside\left(\frac{1}{3}\pi - t\right) + \left(-40 \cdot \cos\left(\frac{2}{3}\pi - t\right)\right) * Heaviside\left(t - \frac{1}{3}\pi\right) \quad (4.23)$$

$$Y = 40 \cdot \sin(t) \cdot Heaviside\left(\frac{1}{3}\pi - t\right) + (80 \cdot \sin\left(\frac{1}{3}\pi\right) - 40 * \sin(\frac{2}{3}\pi - t)) \cdot Heaviside\left(t - \frac{1}{3}\pi\right) \quad (4.24)$$

The path is presented in figure 30.

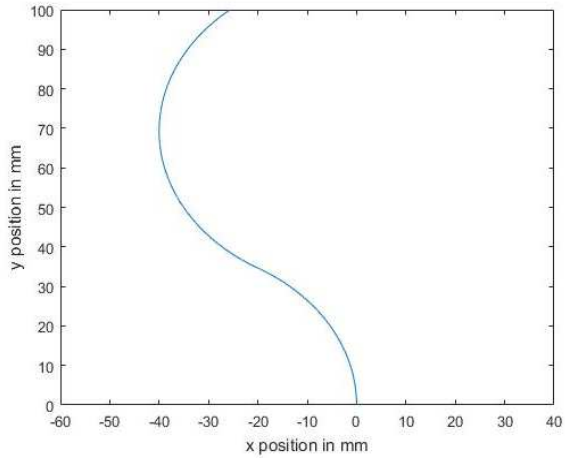

Figure 30: A schematic representation of path case 4 version 1

The second form of this has angles of ½ π. This path can be defined with equations 4.25 and 4.26.

$$X = (40 \cdot \cos(t) - 40) \quad (4.25)$$

$$Y = 40 \cdot \sin(t) \cdot H\left(\frac{1}{2}\pi - t\right) + (80 - 40 \cdot \sin(t)) \cdot H\left(t - \frac{1}{2}\pi\right) \quad (4.26)$$

The equations used in the code are 4.28 and 4.27.

$$X = (40 \cdot \cos(t) - 40) \quad (4.25)$$

$$Y = 40 \cdot \sin(t) \cdot Heaviside\left(\frac{1}{2}\pi - t\right) + (80 - 40 \cdot \sin(t)) \cdot Heaviside\left(t - \frac{1}{2}\pi\right) \quad (4.26)$$

The path is presented in Figure 31.

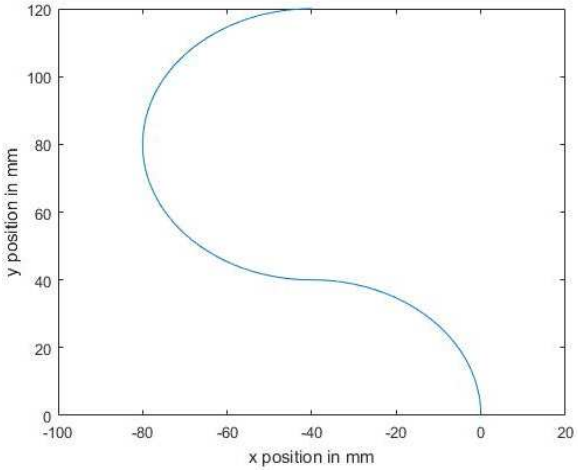

Figure 31: A schematic representation of path case 4 version 2

4.5 Performance evaluation

The performance measurement of the instruments should be as unbiased as possible. A couple limitations of this evaluation should be taken into account.

Limitations

The equations of the paths are always arbitrary. Therefore, it is decided to use two equations for each type of path. This will make the results more diverse, and therefore more reliable. The straight line is only programmed in one-way

because other equations of a straight line will not change the path.

The Step-size influences the accuracy of the instrument. The step-size between starting points can be minimized for the error calculation of the complex segment. To determine the step-size that should be used for this calculation, it is decided to compare results with different step-sizes. Figure 32, 33 and 34 are error plots of case 3.1 sinusoid, and have a step-size of respectively 0.01, 0.005 and 0.001. It can be noticed that the maximal error with a step-size of 0.005 is 0.12mm smaller compared to the maximal error when a step-size of 0.01 is used. This difference is far less than 1% of the maximal excepted error of 3mm. When the step-size 0.005 and 0.001 are compared, it can be noticed that the error only differs with 0.01mm, while the calculation time is increased by a factor 5. Case 2.1 exponential showed a comparable result. Therefore, it is decided to use a step-size of 0.005.

Error measurement

The different instruments are compared based on the error. The error plots that will primarily be used are the normal error plot with the largest and average error, the histogram of the errors, and the plot of the segments over the desired path.

For the determination of the error each configuration should have a number of segments. The number of segments will vary. Firstly, the instrument with parallel cables is placed over the path. The number of segments needed to get the maximal error below 3 mm will be determined. Afterwards, the instrument with parallel and diagonal cables will be placed over the path, with the same amount of DOF so half the amount of segments, and the number of segments that deliver the same maximal error. It should be noted that the maximal error does not need to decrease when the number of segments increases.

The number of segments of the first case, a straight line will deviate from the standard because the case is only a proof of a working algorithm.

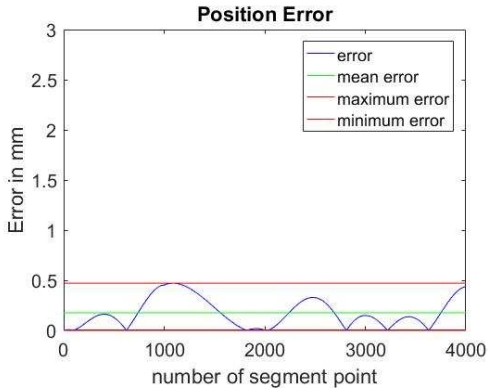

Figure 32: A schematic representation of the error of case 3.1 with a step-size of 0.01.

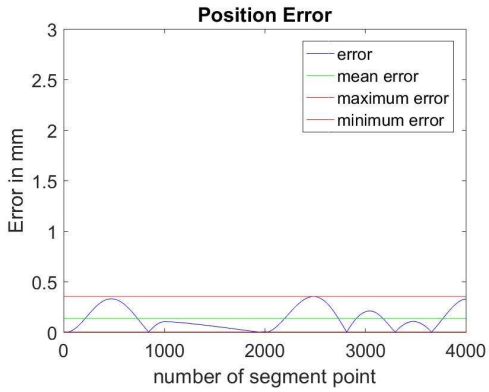

Figure 33: A schematic representation of the error of case 3.1 with a step-size of 0.005.

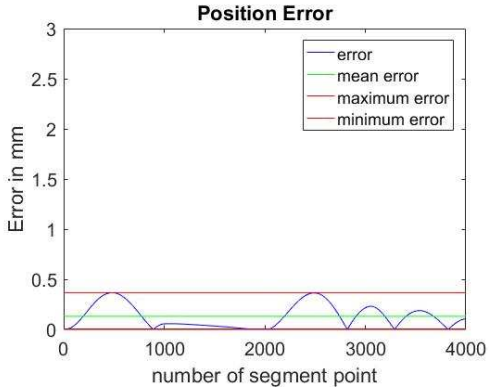

Figure 34: A schematic representation of the error of case 3.1 with a step-size of 0.001.

5. Results and analysis

Intro

This chapter will present the results of the simple and complex instrument following different paths. Afterward the results will be analyzed.

The graphs in the second row of Table 1 to 7 of both the simple and the complex instrument show the desired path and the form of the instrument. The instrument consists of segments, which are colored red and green, depending on the position of the segment. The bottom segment is always colored red, the attached segment is colored green, the next segment is again red and so on. The scale next to the axis is a position scale in mm.

The third row of Table 1 to 7 shows the distance of the instrument compared to the ideal path. The instrument is represented with 4000 points. These points are equally distributed among the instrument. The distance from those points to the path are measured and plotted in this graph. The vertical axis shows the size of the error, while the horizontal axis shows the number of the segment point. The first segment point can be found on the basis of the instrument. Point 4000 is at the tip of the instrument. The red line shows the minimal and maximal error. And the green line shows the average error. The blue line shows the error for each point.

The histogram plot, the fourth row of Table 1 to 7, shows the same errors as the previous plot. This plot orders the errors in their size. This gives a better overview of the errors.

The error table, the fifth row of Table 1 to 7, shows the difference between the endpoint of each segment and the desired end positions of each segment.

5.1 Case 1 straight

The simple and the complex instrument show that they are capable of following a straight line with one or multiple segments. For the test, four segments are used. Because this will also show insight in the connection between segments. The results of case 1 are presented in Table 1.

Instrument and path plot

In these particular graphs of Table 1 row 2, the instruments completely overlap the path. This shows that the instruments are at least quite capable of forming the desired path. Keep in mind that the graphs are relatively small, and small errors and other details are hard to notice on this graph.

Error position plot

Table 1 row 3 shows that the instruments are capable of approaching the desired path with a high accuracy. Therefore the position error of the instruments is negligible. Notice that the scale in the simple segment is in the order of 10^{-11}, this would equal the scale of ten femtometer. The error scale of the complex segment is in the order of 10^{-4}, which equals the scale of a hundred nanometer. Although it looks like the error of the simple segment is rapidly increasing, the error is so small it should not be taken into account. The complex instrument shows that the error goes to zero a couple of times in the graph. This happens when the complex instrument crosses the desired path. Whenever the desired path is crossed, the instrument technically lays on the path, therefore the error is close to zero. Both instruments can form a straight line, so the calculated error is only due to the accuracy of the error calculation.

Histogram error plot

Table 1 row 4 shows that the errors are incredibly small. Therefore this plot only shows

that both instruments are capable of following the path.

Error table

Those errors are below 500 nanometer and therefore the tables do only show zeros.

In practice

Although the instruments are in practice capable of forming a straight line, the accuracy will not approach the accuracy of the algorithm, due to the accuracy of the production, and Elastic modulus of the cables. Both instruments are capable of following a straight-line with a high accuracy.

Table 1: Case 1. Straight line. The second row shows two path plots as well as the instrument following the path. The third row shows an error plot. The fourth row shows a histogram of the error plot. And the fifth row shows the endpoint errors of the segments compared to the desired position.

The simple instrument Case 1	The complex instrument Case 1
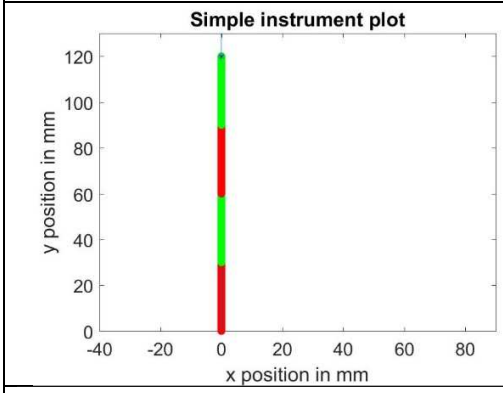	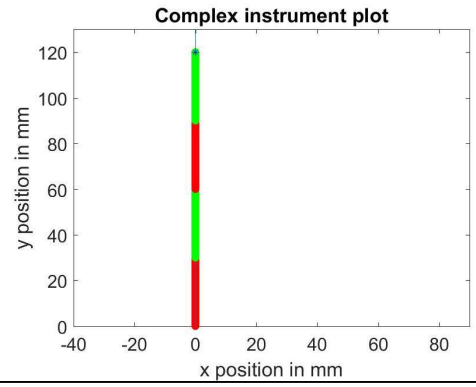
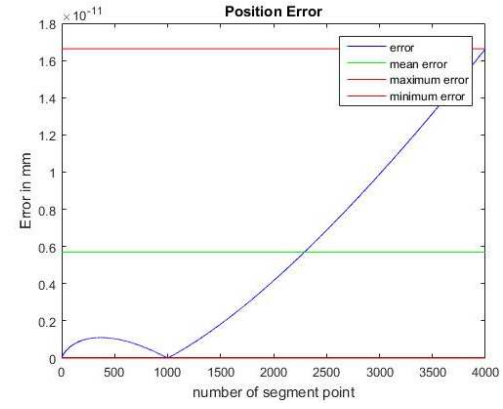	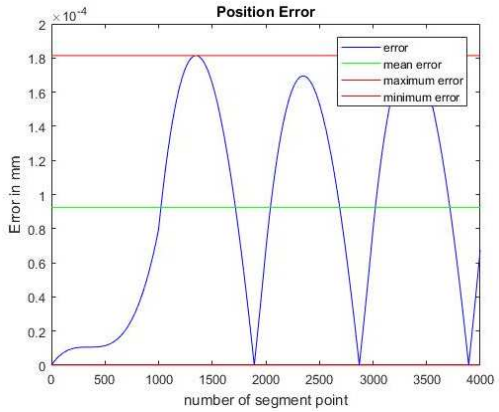
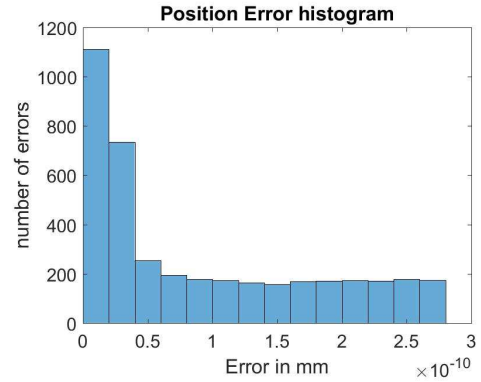	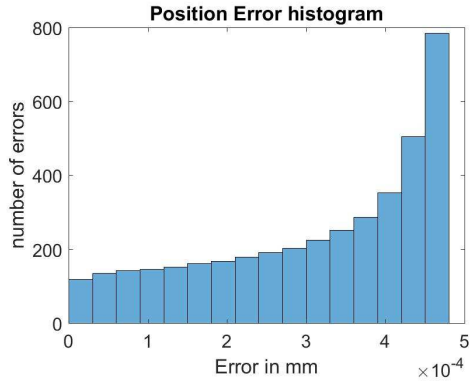

Error of the end position compared to the desired position (simple)

Segment	**1**	**2**	**3**	**4**
Error mm	0.000	0.000	0.000	0.000

Error of the end position compared to the desired position (complex)

Segment	**1**	**2**	**3**	**4**
Error mm	0.000	0.000	0.000	0.000

5.2 Case 2 exponential

Case 2 consists of two different types of exponential equations. These preformed paths are followed by the simple instrument and by the complex instrument. Firstly the results of case 2.1 will be analyzed.

5.2.1 Case 2.1

Case 2.1 shows an exponential path with a relatively blunt bend. This path should be easier to follow than case 2.2. The results of case 2.1 are presented in Table 2.

Instrument and path plot

The Simple instrument is able to follow the exponential path with 3 segments and a maximal error of 3 mm. However, the path is clearly not covered by the instrument, see row 2 of Table 2. So the instrument has a continuous error.

Notice that it is not possible to form a complex instrument with the same amount of DOF, as the simple instrument. Therefore there it was decided to plot a complex instrument with 4 DOF, one more than the simple instrument, and a complex instrument with 2 DOF, one less than the simple instrument.

The complex instrument with two segments and four DOF is overlapping the path in the instrument and path plot. Thus it is relatively accurate in following the path. See Table 2 row 2.

The complex instrument with one segment and two DOF is not totally overlapping the path. It can be noticed that the instrument is moving away from the path in the middle of the segment. But the tip finds the ideal path again.

Error position plot

The simple segment shows an error that is increasing at the start of the instrument, see Table 2, row 3. After a rapid increase, the error seems to be stable. Notice that the instrument is not capable of optimizing to a position.

The complex instrument with two segments shows a maximal error below 0.15 mm. This is fairly accurate. Definitely compared to the simple instrument, with a maximal error just below the 2.5 mm. It can be noticed that the instrument crosses the path multiple times, therefore the error position plot shows multiple zeros. The error seems relatively large at the end of the first segment. The segment does, however, not optimize to the minimal distance to the path, but only to the minimal distance to the desired endpoint.

The complex instrument with one segment shows an error at the center of the segment that is higher than the maximal error of the simple segment. However, this error is compensated at the end of the segment. This suggests that the instrument is more capable of following the path than the simple instrument. Additionally the average error is also smaller.

Histogram error plot

The histogram of the simple instrument shows a high amount of relatively large errors. The complex segment with two segments does not show large errors. The complex instrument with one segment is showing a high number of small and a high number of large errors.

Error table

The endpoints of the simple instrument are clearly further from the desired endpoints than the endpoints of the complex instruments. The endpoint error of the simple instrument is also increasing. This can be explained because the instrument does not have information about the position of the desired endpoint. And therefore cannot optimize to this point, or compensate for previous errors.

In practice

he results show that a complex instrument with two segments is much better at approaching the path than the simple instrument is. However, this complex segment would also have one DOF more. A complex instrument with one segment also seems to be more capable of approaching

Table 2: Case 2.1. An exponential equation. The second row shows three path plots as well as the instrument following the path. The third row shows an error plot. The fourth row shows a histogram of the error plot. And the fifth row shows the endpoint errors of the segments compared to the desired position.

The simple instrument Case 2.1	The complex instrument Case 2.1, same amount of DOF	The complex instrument Case 2.1, same maximal error
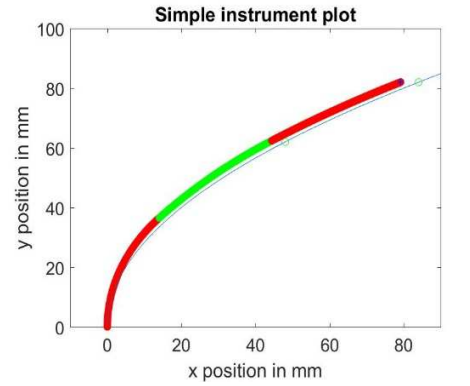	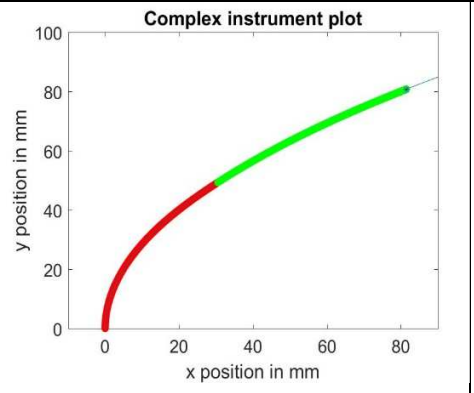	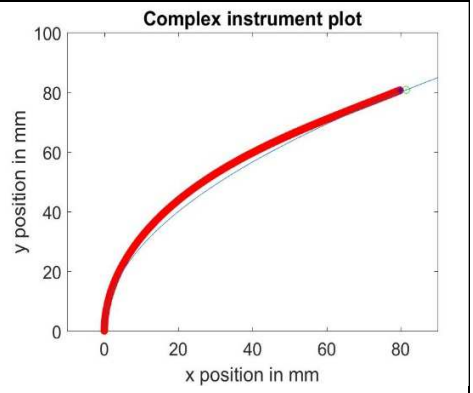
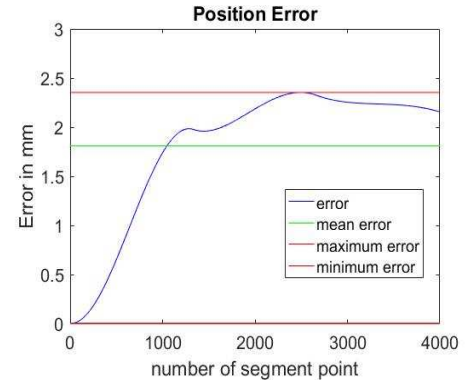	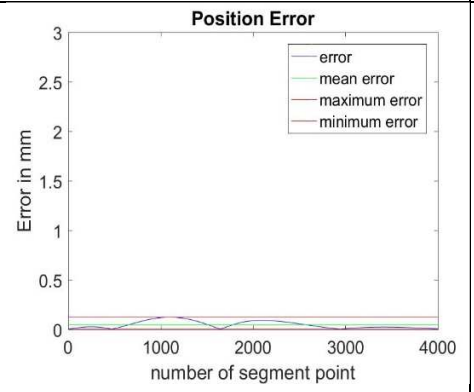	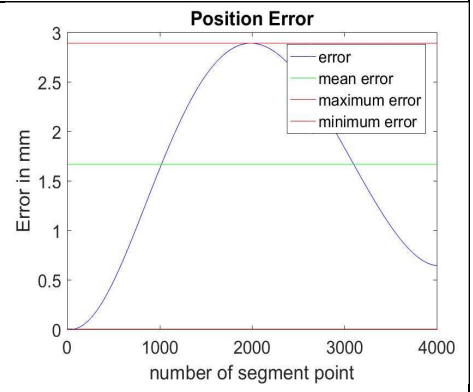
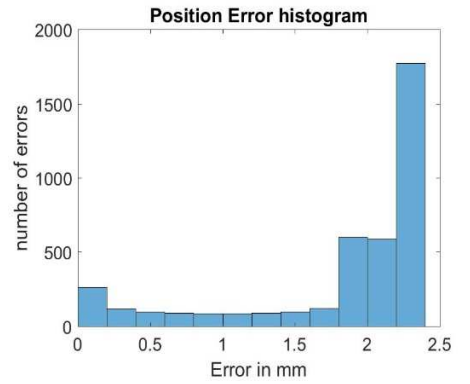	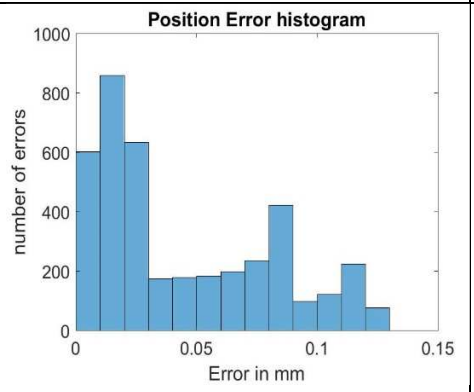	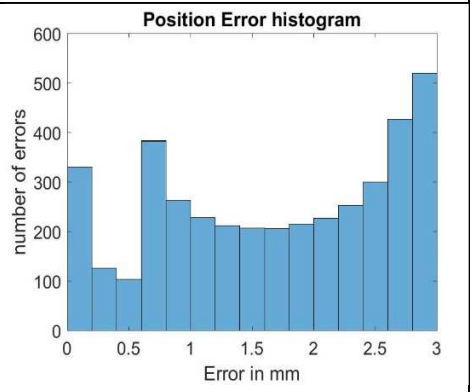
Error of the end position compared to the desired position (simple) *Segment* | **1** | **2** | **3** *Error mm* | 2.248 | 3.694 | 4.852	*Error of the end position compared to the desired position (complex)* *Segment* | **1** | **2** *Error mm* | 0.1354 | 0.0114	*Error of the end position compared to the desired position (complex)* *Segment* | **1** *Error mm* | 1.545

the desired path. Although the maximal position error is larger, the tip error is smaller, and the average position error is also smaller. In practice a segment of 120 mm seems relatively long. But one segment is probably easier to produce than 3 simple segments mounted together.

5.2.2 Case 2.2

Case 2.2 shows an exponential path with a relatively sharp curve at the start of the path. Therefore the start of the path is hard to approach. The results are presented in Table 3.

Instrument and path plot

The Simple instrument is able to follow the exponential path with 8 segments and a maximal error of 3 mm, see Table 3 row 2. This is a relatively high number of segments, besides the path is still not covered at the difficult part.

A complex instrument with four segments and the same amount of DOF as the simple segments seems to cover the path more decently.

A complex instrument with three segments and a maximal error below 3 mm seems to overshoot at the first curve. Afterwards, this overshoot is compensated.

Error position plot

The simple instrument shows a large error at the start of the instrument. This peak is just after the end of the first segment. This was expected because this curve is the hardest part of the path to follow. The simple instrument is, capable of reducing the error to a minimum after the sharp curve.

The complex instrument with four segments has a smaller maximum error of 1.5 mm, instead of 2.4 mm of the simple instrument. However, this difference is small compared to the other cases. This means that the instrument is only slightly better at following this track. This is probably because the end position of the first segment is already past the difficult curve. So this information cannot be used for the reduction of the maximal error.

The results of the complex instrument with 3 segments are comparable to the result of the complex instrument with 4 segments. However, the error is larger. The error is in the same range as the error of the simple instrument.

Histogram error plot

All of the instruments show relatively few large errors and a large number of small errors. This is the case because the path is only difficult to follow at the start.

Error table

The endpoint errors of the simple instrument compared to the desired points are very large compared to the complex segment. This shows that the instrument is not able to follow the path. Although the error plot shows that the instrument is overlapping the path, the desired points are far from reach. Thus the information retrieved from the desired points is only correct because the angles between the desired points are approximately the same.

The error table clearly shows that the complex instrument with four segments is better at approaching the desired position, overall the error is around 50% smaller compared to the complex instrument with three segments.

In practice

The sharp angle at the start of the path might be hard or impossible to follow with the produced segments in practice. However, it is interesting to see that both segments are able to follow a straight line after a sharp angle. However, the simple segment is not able to find the path with

a high accuracy after the difficult angle. While both complex instruments reduce their error drastically after the difficult angle. This is the case because the simple instrument can only optimize to an angle and not to a position. This restriction is clearly visible, and definitely a huge loss. The simple instrument is lacking the capability of reducing a previous error, while the complex segment can reduce a previous error.

Table 3: Case 2.2. An exponential equation. The second row shows three path plots as well as the instrument following the path. The third row shows an error plot. The fourth row shows a histogram of the error plot. And the fifth row shows the endpoint errors of the segments compared to the desired position.

The simple instrument Case 2.2	The complex instrument Case 2.2, same amount of DOF	The complex instrument Case 2.2, same maximal error
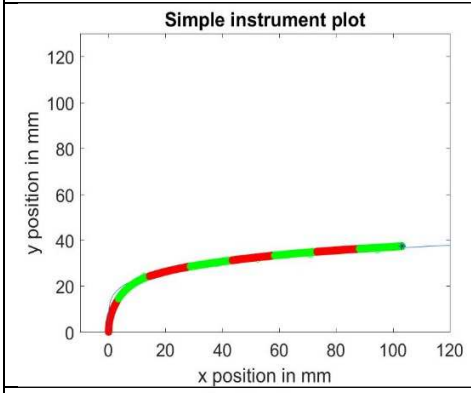	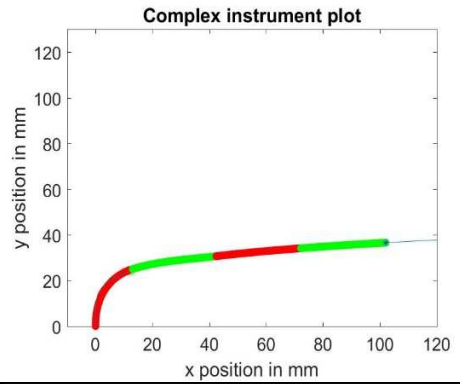	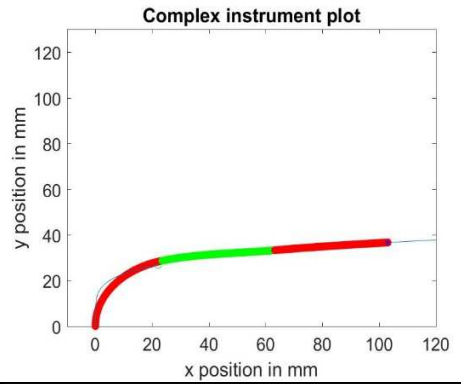
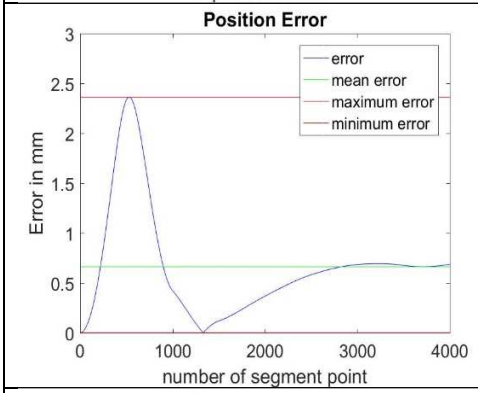	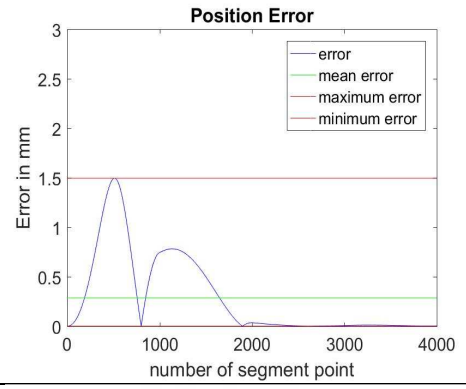	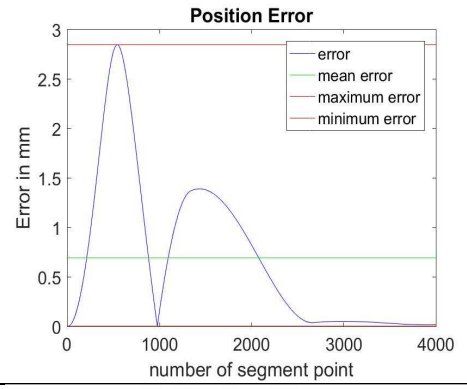
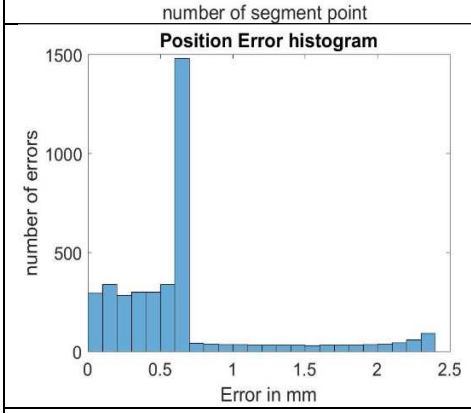	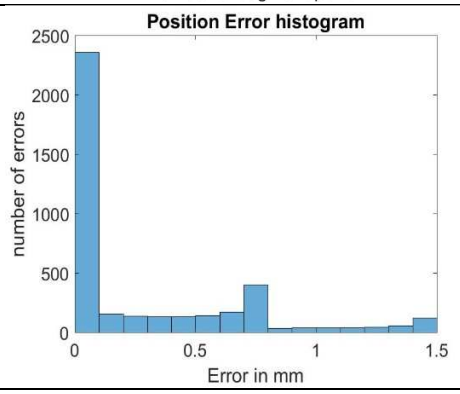	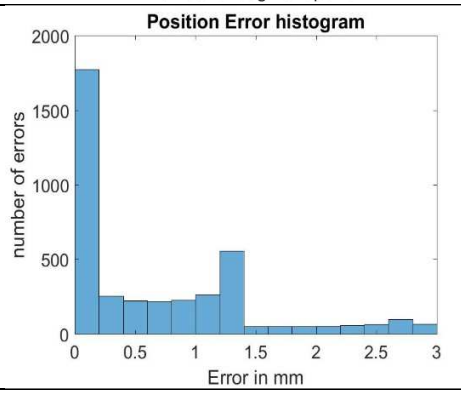

Error of the end position compared to the desired position (simple)

Segment	**1**	**2**	**3**	**4**
Error mm	2.412	1.962	1.932	5.671
Segment	**5**	**6**	**7**	**8**
Error mm	6.073	2.456	6.260	8.801

Error of the end position compared to the desired position (complex)

Segment	**1**	**2**	**3**	**4**
Error mm	1.082	0.564	0.510	0.527

Error of the end position compared to the desired position (complex)

Segment	**1**	**2**	**3**
Error mm	2.149	0.949	0.997

5.3 Case 3 sinusoid

Case 3 is two sinusoids. These paths are relatively hard to follow because the paths have multiple curves. Case 3.1 shows a sinusoid with relatively soft bends, where 3.2 has more and sharper curves and is therefore even more challenging.

5.3.1 Case 3.1

Case 3.1 shows a sinusoid, with relatively blunt bends. Multiple curves make the path harder to follow. The results are presented in Table 4.

Instrument and path plot

The simple instrument needs eight segments to follow the path, see row two Table 4. And even with eight segments, it is still clear to see that the second curve is hard to form.

The complex instrument seems to perform much better with the same amount of DOF. Notice that the path seems completely covered by the segments.

The complex instrument with three segments is able to follow the path with a maximum error below 3 mm, even below 1 mm. However, this path can no longer be followed with 2 segments.

Error position plot

The error position plot of the simple instrument shows the error at the second curve as the maximal error, as expected. The error seems to be recovered at the tip of the instrument, this is however, a coincidence.

The complex instrument with four segments shows a relatively small error below 0.4 mm. An order of magnitude smaller than the simple instrument.

The complex instrument with three segments is also outperforming the simple instrument. The maximal error is around 1 mm. So it is safe to say that the complex instruments are performing much better on this complex path.

Histogram error plot

The histogram shows that the simple instrument only has a few large errors. The modulus lays between 0.8 and 0.9 mm. This is still large compared to the complex instruments. The complex instruments have a more evenly distributed error, also due to the smaller errors.

Error table

The error table clearly shows that the complex instruments are better in approaching the desired positions, compared to the simple instrument. The simple instrument shows errors between the 1.1 mm and 3.2 mm, while the maximal error of the complex instruments is 0.75 mm. Thus the simple instruments performed significantly worse in following the desired path.

The error table clearly shows that the complex instrument with four segments is better at approaching the desired position, overall the error is around 50% smaller compared to the complex instrument with three segments.

In practice

The simple instrument clearly has more difficulties following a complex sinusoid path, compared to the complex instruments. The average and maximum error are much higher, even with more DOF. For this specific path, it is safe to say that the complex instrument is outperforming the simple instrument on all fronts.

Table 4: Case 3.1. A sinusoid. The second row shows three path plots as well as the instrument following the path. The third row shows an error plot. The fourth row shows a histogram of the error plot. And the fifth row shows the endpoint errors of the segments compared to the desired position.

The simple instrument Case 3.1	The complex instrument Case 3.1, same amount of DOF	The complex instrument Case 3.1, same maximal error
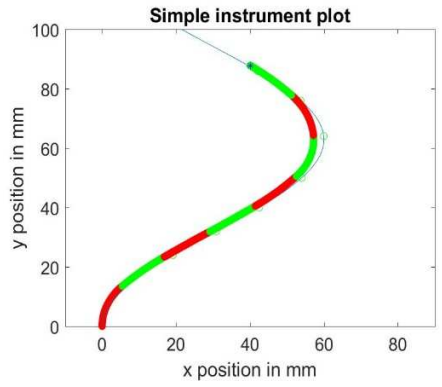	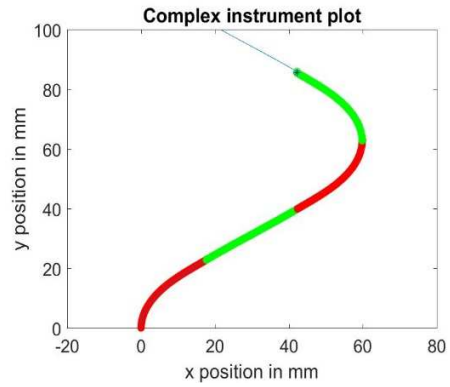	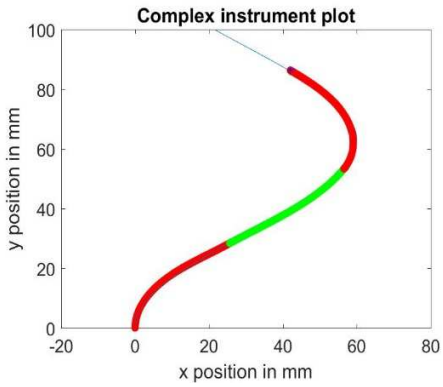
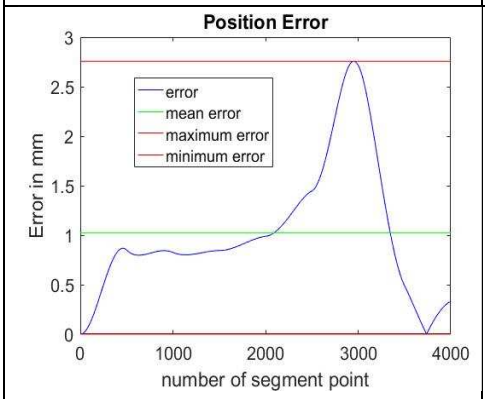	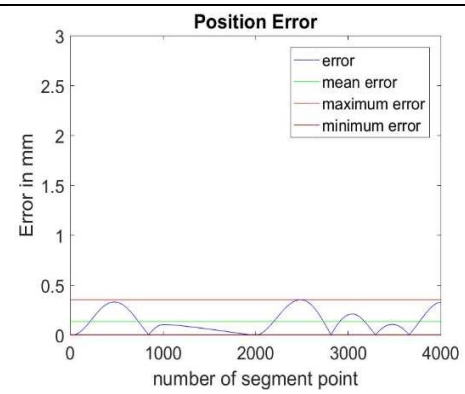	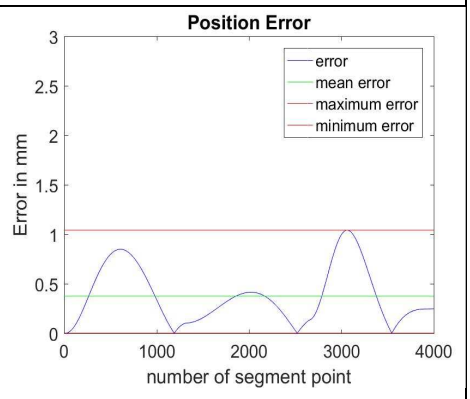
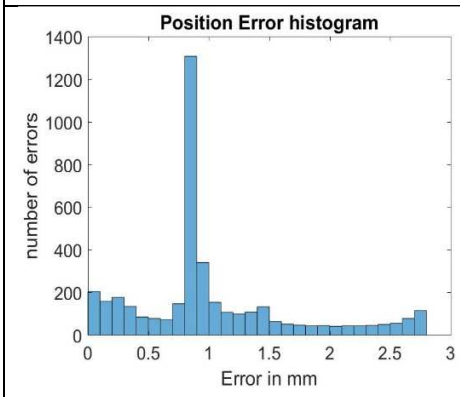	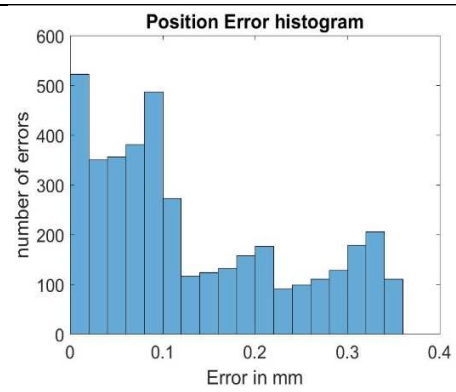	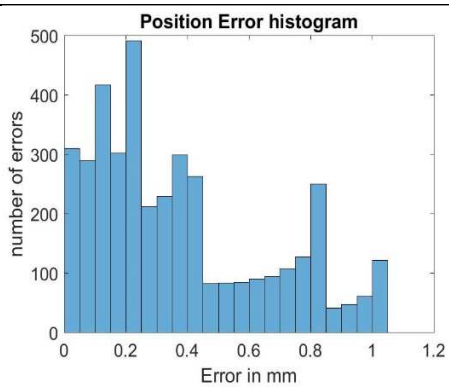
Error of the end position compared to the desired position (simple) *Segment* | **1** | **2** | **3** | **4** *Error mm* | 1.629 | 2.392 | 1.712 | 1.130 *Segment* | **5** | **6** | **7** | **8** *Error mm* | 1.569 | 2.799 | 3.102 | 2.673	*Error of the end position compared to the desired position (complex)* *Segment* | **1** | **2** | **3** | **4** *Error mm* | 0.202 | 0.141 | 0.289 | 0.298	*Error of the end position compared to the desired position (complex)* *Segment* | **1** | **2** | **3** *Error mm* | 0.418 | 0.484 | 0.753

5.3.2 Case 3.2

The second sinusoid, case 3.2 is a difficult path with multiple changes of direction. This path is really challenging due to the number and sharpness of the bends. This path is the most complex variant, and can probably not be followed in practice due to the sharp bends. However, the results still give insight in the maneuverability of the different instruments. The results are presented in Table 5.

Instrument and path plot

The simple instrument needs fifteen segments to follow this path, see Table 5 row 2. This is an extreme amount of segments, and therefore hard to manufacture. Even with this number of segments, the error increases at the tip. Because the instrument is not able to correct the previous error.

A complex instrument with seven segments, note that this is one DOF less than the simple instrument, is clearly outperforming the simple instrument. The instrument is capable of completely overlaying the path.

A complex instrument with five segments can follow the path, however, the bends of certain segments are relatively sharp. This might lead to difficulties in practice.

Error position plot

The simple instrument has a sharp bend at the tip. It is not able to reduce this error. It also shows a large error at the second angle.

The complex instrument with seven segments shows fluctuating errors, but all the errors are below 0.45 mm. So the instrument performs well.

The complex instrument with five segments also shows sharp bends at the tip. This is probably due to the complexity of the second angle. The instrument should, in contradiction to the simple instrument, be able to reduce this error when the instrument follows the path even further.

Histogram error plot

The histogram plots from all of the instrument show a relatively low number of large errors.

Error table

The simple instrument performs worse in reaching the desired points compared to the complex instrument with the same amount of DOF. However, the complex segment with the same error also shows one large error at the tip, compared to the desired endpoint. It should also be noted that the desired endpoint error of the simple instrument is not constantly increasing. This is a coincidence because the instrument has no information about the desired position.

The error table clearly shows that the complex instrument with seven segments is better at approaching the desired position than the complex instrument with five segments. An endpoint error at the tip of 2 mm shows that the instrument with five segments is no longer able to follow the path correctly.

In practice

The main conclusion from this path is that the simple instrument performs less well on complex paths. This path is more a proof of concept than a realistic real-life measurement. Due to the sharp curves, and the lack of a maximal segment angle, the bending of certain segments is really high. The high number of segments needed by the simple instrument makes it also hard to fabricate. So the path is certainly complex to follow with both methods.

The path is, however, still interesting because it shows the potential possibilities of both cable configurations. The potential possibilities of the

segments with parallel and diagonal cables seem much higher, than the possibility of an instrument based on only parallel cables, in complex paths.

Table 5: Case 3.2. A sinusoid. The second row shows three path plots as well as the instrument following the path. The third row shows an error plot. The fourth row shows a histogram of the error plot. And the fifth row shows the endpoint errors of the segments compared to the desired position.

The simple instrument Case 3.2	The complex instrument Case 3.2, same amount of DOF	The complex instrument Case 3.2, same maximal error
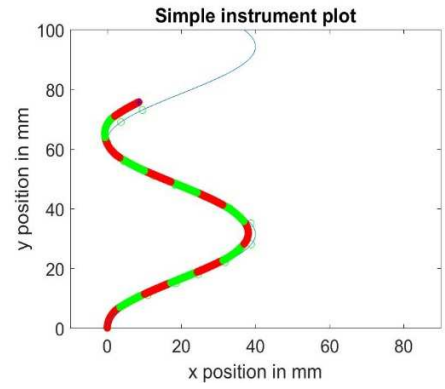	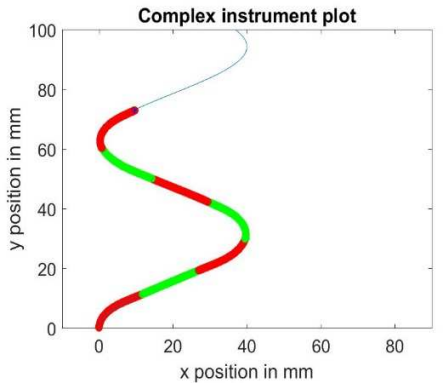	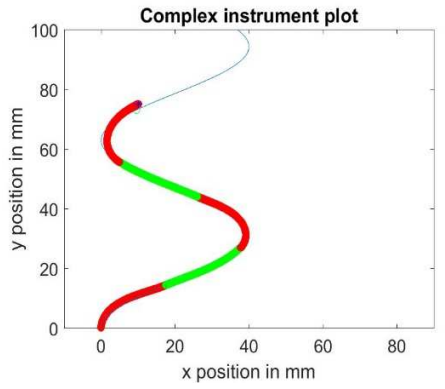
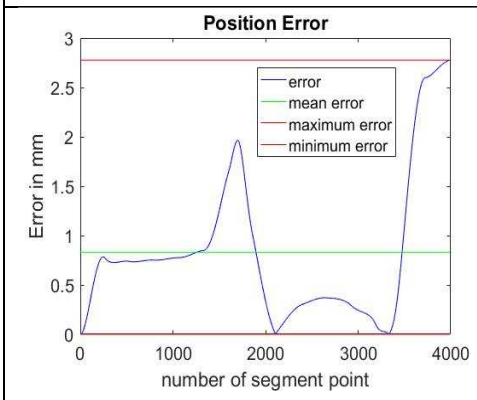	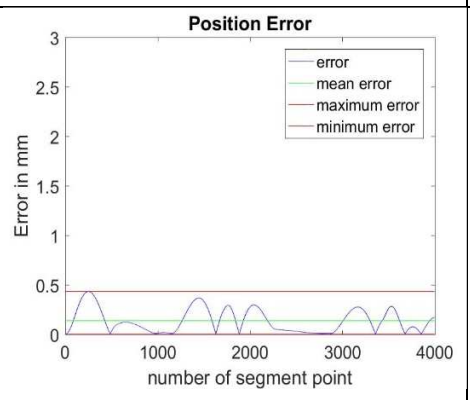	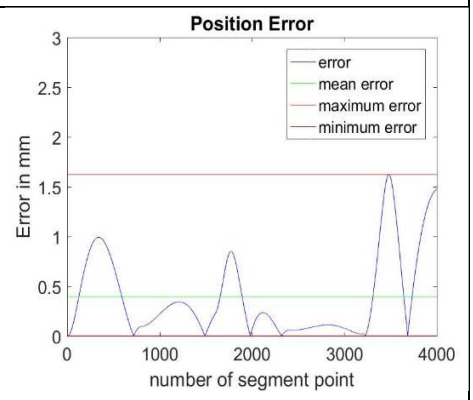
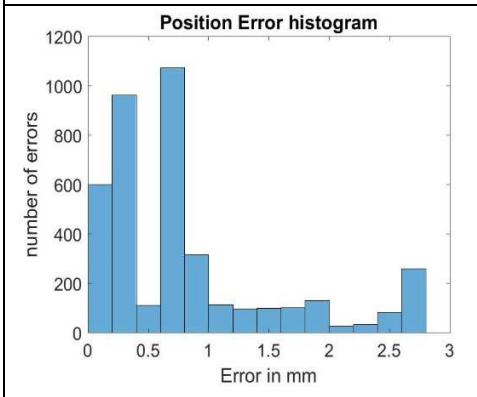	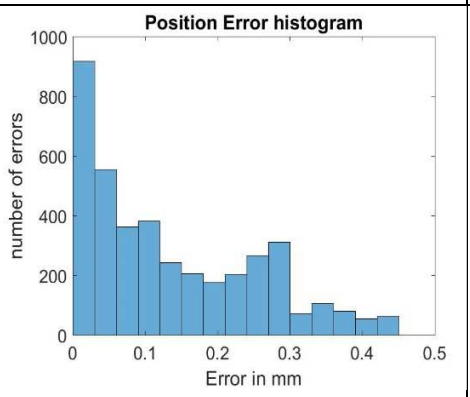	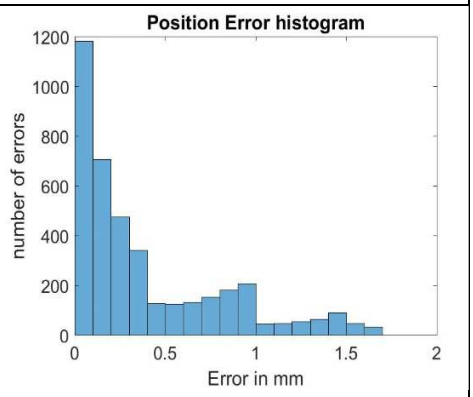

Error of the end position compared to the desired position (simple)

Segment	**1**	**2**	**3**	**4**
Error mm	1.306	0.940	1.465	0.781
Segment	**5**	**6**	**7**	**8**
Error mm	0.857	1.914	1.997	2.284
Segment	**9**	**10**	**11**	**12**
Error mm	2.288	1.460	2.902	1.525
Segment	**13**	**14**	**15**	
Error mm	1.908	2.599	2.821	

Error of the end position compared to the desired position (complex)

Segment	**1**	**2**	**3**	**4**
Error mm	0.260	0.217	0.376	0.244
Segment	**5**	**6**	**7**	
Error mm	0.241	0.328	0.153	

Error of the end position compared to the desired position (complex)

Segment	**1**	**2**	**3**	**4**
Error mm	0.555	0.613	0.219	0.078
Segment	**5**			
Error mm	2.058			

5.4 Case 4 circular arcs

Case 4 describes a path consisting of two parts with a constant curvature, so parts of a circle. These paths are consisting of two parts with a constant curvature and seem easy to follow. Because an instrument is able to form a constant curvature, it can follow a constant curvature line. However, the shape in this case consists of two different arcs. This will result in some difficulties at the point where the radius of curvature switches.

5.4.1 Case 4.1

The curve of the first case has an angle up to 1/3π. The second part is defined by the same radius of curvature, in the opposite direction. The results of case 4.1 are presented in Table 6.

Instrument and path plot

The simple instrument needs 5 segments to follow the path with a maximal error below 3 mm, see Table 6 row 2. Notice that the instrument follows the desired path perfectly for the first segment. This is possible because the path is a constant curvature. However, the path between the end point of the first segment and the end point of the second segment has no longer a constant curvature. So after the second segment, an error starts to form.

It is not possible to reach five DOF with the complex instruments. Therefore, there is decided to plot an instrument with six DOF and one with four DOF. An instrument with six DOF seems completely capable of following the path. An instrument with four DOF shows, however, some errors at the first angle.

Error position plot

The error plot shows that the simple instrument is perfectly capable of following the path for the first segment. Afterwards, an error is introduced. Although it looks like the error is compensated, this is not the case. The instrument simply crosses the desired path, this reduces the distance between the instrument and the desired path.

The complex instrument with three segments shows a maximal error below 0.5 mm. But it should be taken into account that this instrument uses more DOF than the simple instrument. A simple instrument with 6 segments, shows an error just above 0.8 mm to put the results in context.

The complex instrument with two segments shows a comparable maximum error as the simple instrument with one DOF more.

Histogram error plot

The histogram plots from all of the instruments show a high number of small errors. The results are in line with the expectations, given the results of the previous plots.

Error table

The error table of the simple instrument shows that the desired position of the first segment is reached exactly. This is because the start of the path has a constant curvature. After the first segment, a small error occurs, this is because the second part does not have a constant curvature. Afterwards, the error stays constant. This is expected because the curvature is again constant after the second segment.

The complex segments do not show a zero error because the segment covers a larger part of the path. This larger part does not have a constant curvature. However, both the instrument with 3 as the instrument with 2 segments is capable of correcting for the error.

In practice

The path is not extremely difficult to follow and does not show sharp bends. However, the complex instrument with only two segments might give trouble with the relatively sharp angles per segment.

Table 6: Case 4.1. An equation existing of constant curvature arcs. The second row shows three path plots as well as the instrument following the path. The third row shows an error plot. The fourth row shows a histogram of the error plot. And the fifth row shows the endpoint errors of the segments compared to the desired position.

The simple instrument Case 4.1	The complex instrument Case 4.1, same amount of DOF	The complex instrument Case 4.1, same maximal error
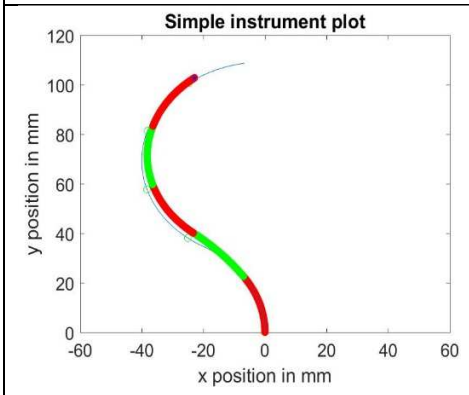	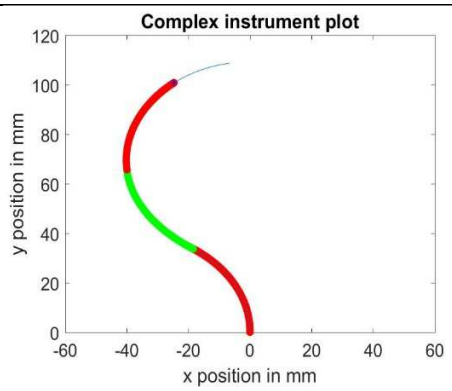	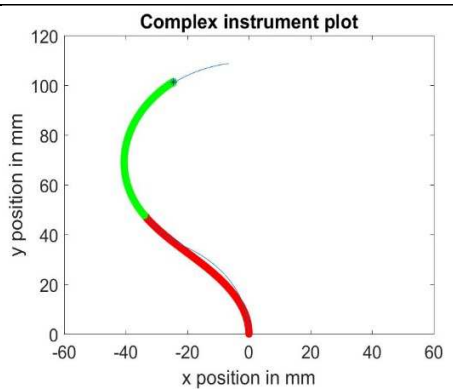
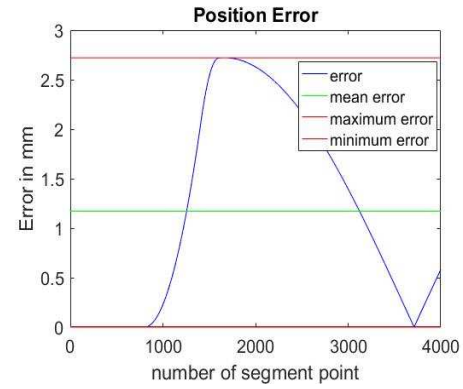	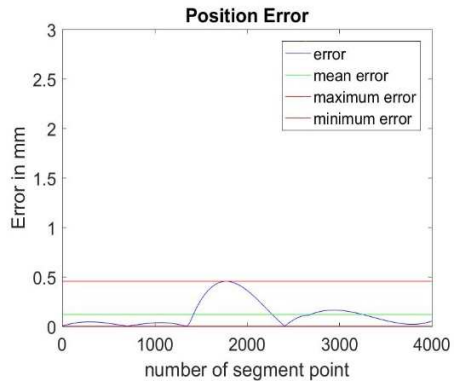	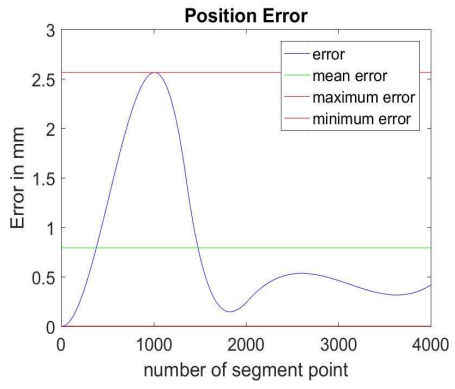
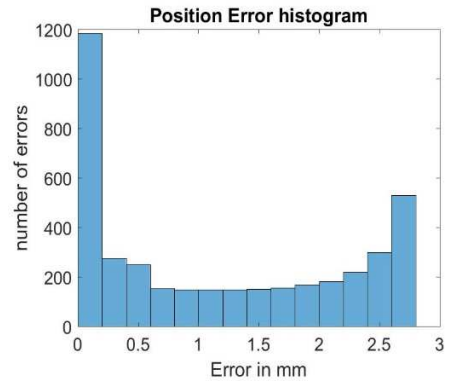	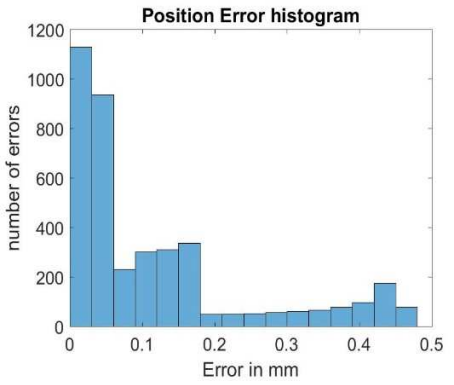	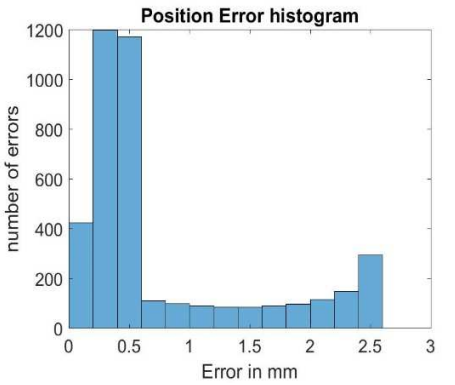
Error of the end position compared to the desired position (simple) *Segment* | **1** | **2** | **3** | **4** *Error mm* | 0.000 | 2.722 | 2.722 | 2.722 *Segment* | **5** *Error mm* | 2.722	*Error of the end position compared to the desired position (complex)* *Segment* | **1** | **2** | **3** *Error mm* | 0.045 | 0.169 | 0.047	*Error of the end position compared to the desired position (complex)* *Segment* | **1** | **2** *Error mm* | 1.057 | 0.646

The complex instruments show clear advantages in the error table. This simply shows that the complex instrument is better at reaching the desired end position. And shows the importance of compensating an error. Even in a constant curvature path with only one change of direction, the simple instrument will still show a large error and is unable to compensate for this error.

5.4.2 Case 4.2

The second version of case 4 shows an arc with a constant curvature up to an angle of ½ π before the curvature changes in the opposite direction. The results of case 4.2 are presented in Table 7.

Instrument and path plot

The simple instrument needs 6 segments to follow the path with a maximal error of 3 mm. Notice that the instrument is capable of following the path nicely.

The complex instrument with the same amount of DOF is also perfectly capable of following the path. The same goes for the complex instrument with two segments.

Error position plot

The simple instrument shows that the error is close to zero for the first 3 segments. This is the case because the curvature is constant. Afterwards, the maximal error occurs, that is below 1.2 mm. This is small compared to other cases because a simple instrument with 5 segments shows a maximal error just above the 3.5 mm.

The complex instrument with three segments shows an even smaller maximum error of 0.75 mm. Although the difference is significant, it is by far not as large as in the previously described cases.

The complex instrument with two segments has a maximum error of 1 mm and is therefore comparable with the error of the simple instrument.

Histogram error plot

The histogram plots from all of the instrument show a relatively low number of large errors.

Error table

The simple segment is perfectly capable of following the first part of the path. This part has a constant curvature. The error is equal to zero for the first three segments. The fourth segment cannot follow a part of the desired path with a constant curvature, so an error occurs. This error cannot be compensated. However, the rest of the path is again a constant curvature, so the error stays the same.

Although the complex instrument is technically capable of following a constant curvature, the way of programming gives a small limitation. To reach a constant curvature the Euler spiral needs to be infinitely long. Therefore a small endpoint error can be noticed for the complex instrument with three segments.

The complex instrument with three segments is capable of reducing the endpoint error. And both complex instruments show a significantly smaller endpoint error than the simple instrument.

In practice

The complex instrument with only two segments should be able to follow the path. However, the angle that a single segment needs to make is around ½ π. Therefore an approach of three complex segments seems more logical.

Notice that the simple segments are capable of following a path with constant curvatures perfectly. However, for each part of the desired

path that does not form a constant curvature, an error will occur. Thus this error will always occur, unless the path is only consisting of one arc with a constant curvature. And this error cannot be compensated. This shows the absolute main disadvantage of the simple instrument.

Table 7: Case 4.2. An equation existing of constant curvature arcs. The second row shows three path plots as well as the instrument following the path. The third row shows an error plot. The fourth row shows a histogram of the error plot. And the fifth row shows the endpoint errors of the segments compared to the desired position.

The simple instrument Case 4.2	The complex instrument Case 4.2, same amount of DOF	The complex instrument Case 4.2, same maximal error
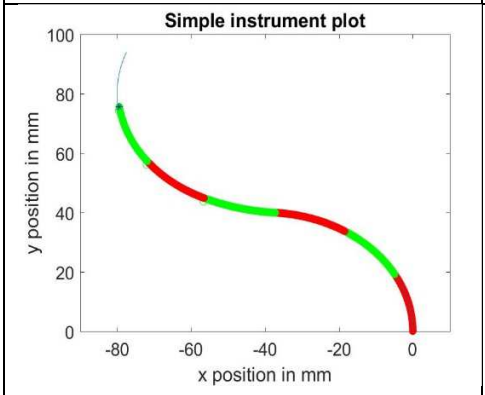	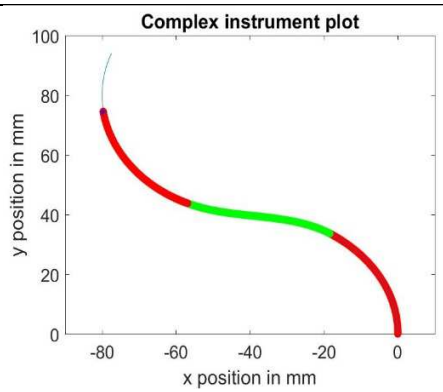	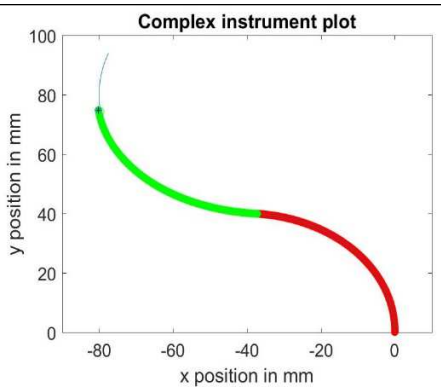
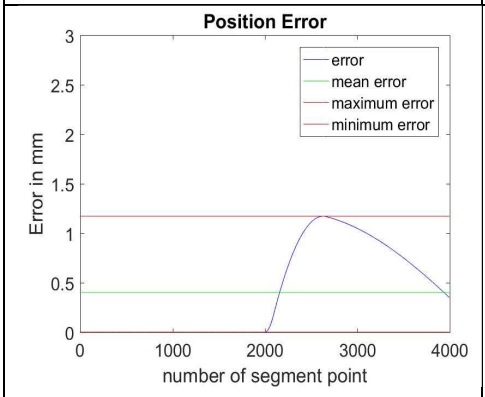	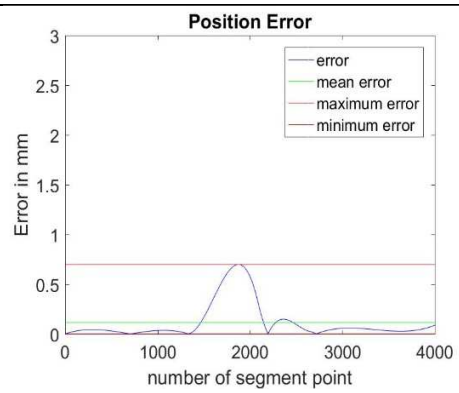	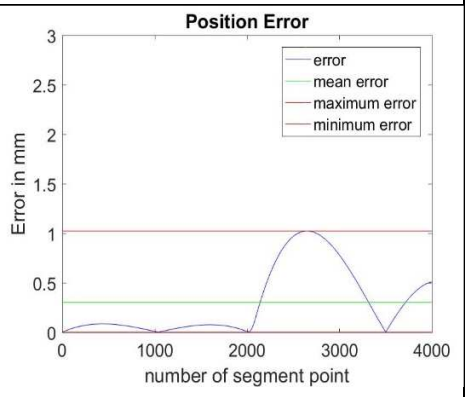
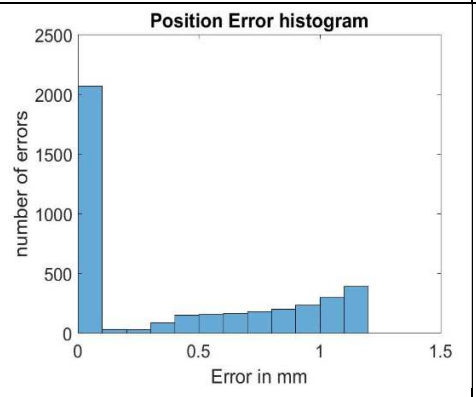	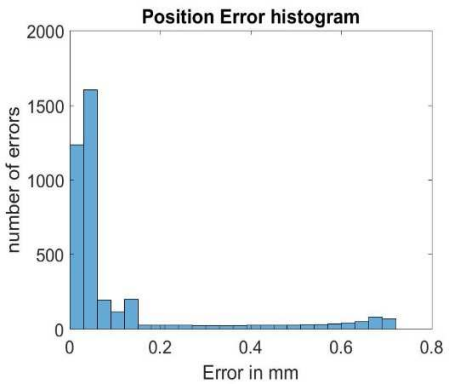	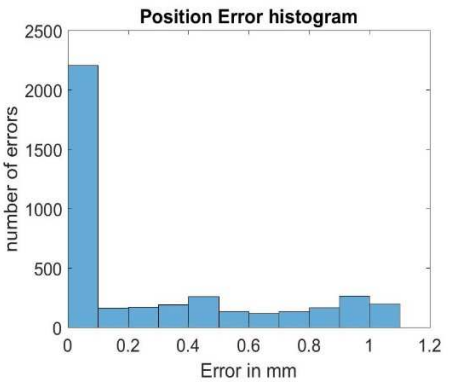
Error of the end position compared to the desired position (simple) *Segment* | **1** | **2** | **3** | **4** *Error mm* | 0.000 | 0.000 | 0.000 | 1.210 *Segment* | **5** | **6** *Error mm* | 1.210 | 1.210	*Error of the end position compared to the desired position (complex)* *Segment* | **1** | **2** | **3** *Error mm* | 0.045 | 0.168 | 0.005	*Error of the end position compared to the desired position (complex)* *Segment* | **1** | **2** *Error mm* | 0.052 | 0.673

5.5 Overview of the results

This section discusses the performance of different instruments on multiple different paths. The results of the different cases deliver information on the behavior of the different instruments. However, one case cannot provide all the information on the instruments, therefore multiple cases were used. This Section will give an overview of the information concluded from the previous results.

It should be kept in mind that all the previously described cases are arbitrary examples of different paths. Besides, the cases do not show a moving instrument, but only an instrument after it has traveled along the path for 120 mm.

Complex instrument with the same amount of degrees of freedom

Whenever the simple instrument is compared to the complex instrument with the same amount of DOF, it should be noticed that the complex instrument is showing smaller errors in all the cases, except for the straight-line, case 1.

Case 1 is a straight-line and both instruments can follow the path exactly. However, the simple instrument is programmed with a possibility of making an arc with a zero angle, this results in a straight-line. The Complex instrument will select a starting point and an endpoint on the Euler spiral and scales the Euler spiral by a massive factor, so a straight-line occurs. Thus the advantages of the simple segment lay in a way of programming.

Whenever the simple instrument is compared to the complex instrument with the same amount of DOF, it can be noticed that the complex instrument is showing smaller errors in all the cases, except for the straight-line, case 1.

In case 2 up till case 4 the complex instrument with the same amounts of DOF, is showing a maximal error, far below the error of the simple instrument. The difference between the error of the simple and the complex instrument seems to be the largest for case 3.1, case 3.2 and case 4.1. These examples give a maximal error difference of a factor 5.

Complex instrument with the same maximal error

Table 8 shows the number of segments needed for the simple and the complex instrument to follow the desired path, with a maximal error of 3 mm. The table clearly shows that the complex instrument needs fewer segments, and fewer DOF to follow all of the different paths, within this error margin. The reduction of DOF is 20% in case 4.1, 25% in case 2.2 and 33% in cases 2.1, 3.2 and 4.2. This is a significant decrease in DOF.

Complex paths performance

The more complex paths like the two sinusoids, case 3.1 and 3.2, show a clear preference for the complex instruments. The complex instrument performed better on all paths. However, the more complex a path seems, the better the complex instrument performers relative to the simple instrument.

Compensating for an error

The information provided to the simple and the complex instrument is different. The simple instrument only receives the desired end angles. These end angles match with a certain end position. However, the end angles also dictate a certain end position of the simple segment, which might not match the desired end position of the path.

Table 8: The number of segments and degrees of freedom needed to follow a path.

	Number of segments simple instrument	Number of segments complex instrument	Number of DOF complex instrument
Case 2.1	3	1	2
Case 2.2	8	3	6
Case 3.1	8	3	6
Case 3.2	15	5	10
Case 4.1	5	2	4
Case 4.2	6	2	4

The complex instruments will receive information of an end position and a desired angle at this position. The desired end position is given in the global frame. Thus the end position error of the bottom segment can be compensated by the next segment.

The end angle of a segment controls the starting angle of the next. This will therefore directly influence the direction of the next segment. If the end angle is not given or not reached, the next segment will start in a wrong direction and would, therefore, perform significantly worse.

The desired position is valid information about the segment. The end position of the previous segment determines the starting position of the current segment. But the most important factor of a position is the possibility to compensate for previous position errors.

Curvature analysis

To get a better understanding of the performance of the instruments, curvature plots have been made from the different paths.

Case 1 the straight path shows that the curvature is constant and zero see Figure 32. Thus the straight path can be perfectly followed by the simple and complex instrument with only one segment, as the results prove.

The second case with the exponential equations gives a different result. Both exponential equations show a relatively constant curvature after 60mm, see Figure 32. The first exponential equation shows an almost linear decrease in curvature at the start of the path. This should be relatively easy for the complex segment to follow. The second exponential equation case 2.2 shows, however, a large fluctuation at the start of the path. This fluctuation can only be approached with 2 complex segments in the first 30mm of the path. In practice, the curvature fluctuation cannot be matched but doesn't create a large position error for the complex instrument. The simple instrument needs multiple segments to overcome this fluctuation.

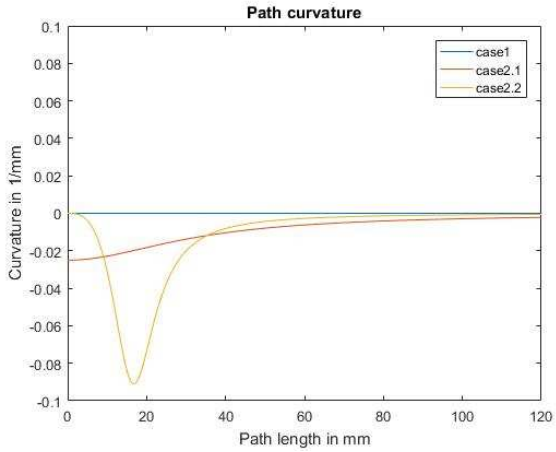

Figure 32: A representation of the curvature of the straight path case 1 and the exponential paths case 2.1 and case 2.2.

The third case with sinusoids does show complex curvature plots. Those plots show that the sinusoid paths are impossible to follow with simple or complex segments and that an approximation requires a large number of

segments. Case 3.1 shows smaller curvature changes and is, therefore, easier to follow, see Figure 33.

The fourth case shows two circular arcs. The direction of the curvature changes after a corner of 1/3π for case 4.1 and after an angle of 1/2π for case 4.2. This switch can be noticed in the curvature plot Figure 34. The curvature plot shows a constant curvature and can, therefore, be followed by both types of instruments. However, the complex instrument is better in handling the switch between the two circular arcs.

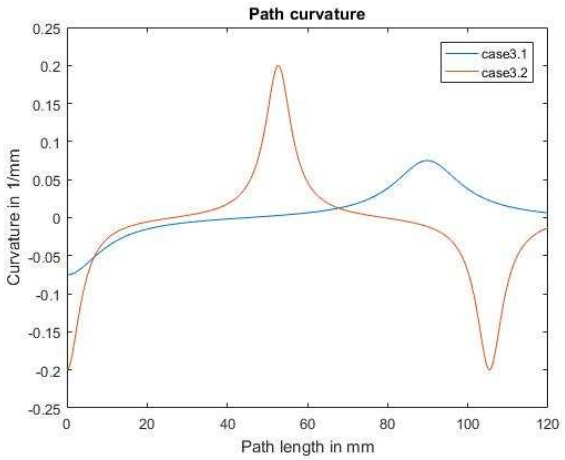

Figure 33: A representation of the curvature of the sinusoid paths case 3.1 and case 3.2.

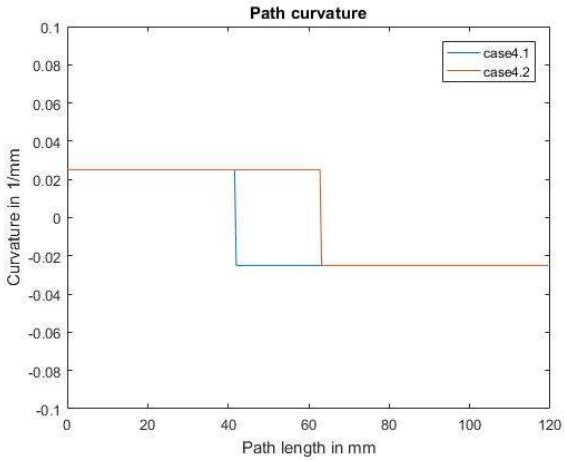

Figure 34: A representation of the curvature of the circular arc paths case 4.1 and case 4.2.

Stability analysis

The stability of the instruments is difficult to calculate. To get an impression of the stability of the results, all the calculated paths are scaled with a factor 0.9 and with a factor 1.1. The maximal error for both the complex and the simple instrument is shown in respectively Table 9 and Table 10. It should be noted that a scaled path will result in different desired positions and therefore will influence the shape of the segments.

Table 9 shows a maximal relative error decrease of 45% and a maximal relative error increase of 173%. It should be noted that this percentage is only a small error increase in mm. The maximal error difference is just below 1.3mm.

Table 10 shows a maximal relative error decrease of 44% and a maximal relative error increase of 116%. The maximal absolute error difference is just below 1.9mm.

Both instruments show relatively large fluctuations whenever the path is 10% larger of 10% smaller than the original form. This means a slightly different path does influence the maximal error significantly for path instruments. This can, however, be explained, because a different path will result in different desired positions and different matching shapes. Table 9 and 10 also show that the complex instrument with the same amount of DOF outperformed the simple instrument on all the cases, also for the scaled paths.

Table 9: The table shows the maximal error of the complex instrument compared to the desired path. The column of 0.9 shows the maximal error whenever the original path is scaled with a factor 0.9. Column 1 shows the maximal error of the original path. And column 1.1 shows the shows the maximal error whenever the original path is scaled with a factor 1.1. The error difference between the two scaled paths and the original path is expressed in percentages in the two right columns.

Case	Number of segments	0.9	1	1.1	(0.9-1)/1 *100%	(1.1-1)/1 *100%
case 2.1	1 segments complex	2.660	2.889	1.677	-8%	-42%
case 2.1	2 segments complex	**0.3296**	**0.1207**	**0.06611**	173%	-45%
case 2.2	3 segments complex	2.882	2.844	2.670	1%	-6%
case 2.2	4 segments complex	**1.806**	**1.495**	**1.126**	21%	-25%
case 3.1	3 segments complex	1.059	1.041	1.888	2%	81%
case 3.1	4 segments complex	**0.6857**	**0.3511**	**0.5502**	95%	57%
Case 3.2	5 segments complex	1.233	1.623	1.937	-24%	19%
Case 3.2	7 segments complex	**1.075**	**0.4319**	**0.8728**	149%	102%
Case 4.1	2 segments complex	2.289	2.564	2.439	-11%	-5%
Case 4.1	3 segments complex	**0.5743**	**0.4526**	**1.030**	27%	128%
Case 4.2	2 segments complex	1.170	1.021	2.295	15%	125%
Case 4.2	3 segments complex	**0.8404**	**0.6989**	**1.125**	20%	60%

Table 10: The table shows the maximal error of the simple instrument compared to the desired path. The column of 0.9 shows the maximal error whenever the original path is scaled with a factor 0.9. Column 1 shows the maximal error of the original path. And column 1.1 shows the shows the maximal error whenever the original path is scaled with a factor 1.1. The error difference between the two scaled paths and the original path is expressed in percentages in the two right columns.

Case	Number of segments	0.9	1	1.1	(0.9-1)/1 *100%	(1.1-1)/1 *100%
Case 2.1	3 segment simple	2.551	2.353	1.607	8%	-32%
Case 2.2	8 segments simple	3.270	2.363	1.377	38%	-42%
Case 3.1	8 segments simple	2.737	2.727	2.965	0%	9%
Case 3.2	15 segments simple	3.157	2.777	2.408	14%	-13%
Case 4.1	5 segments simple	4.590	2.722	1.515	69%	-44%
Case 4.2	6 segments simple	1.764	1.172	2.531	51%	116%

6. Discussion

Intro

The discussion will give a broader interpretation of the results, together with the limitations of the model and the further recommendations.

6.1 Information

The simple instrument receives different information compared to the complex instrument with the same number of DOF. The simple instrument receives end angles, where the complex instrument receives end angles and end positions. A simple segment is capable of reaching the desired angle because the segment has one DOF and the desired angle is one coordinate. The complex segment is, however, not able to reach the desired angle and the desired position, because the desired angle is one coordinate and the desired position is an x and a y-coordinate. So the complex segment is only able to reach the desired angle and optimize to the desired position.

Desired angle

The desired angle is the starting direction of the next segment. If the desired angle is reached, the segment on top of the current segment will start in the desired direction.

The desired angle can also give a hint of the shape of the path between two points. Although this information is less reliable. Whenever the desired path does not consist of a large number of sharp curves, the end angle of a segment will often give an impression of the path between the two desired points. Notice that this information is, however, unreliable.

Desired position

The desired position exist of two coordinates, an x and a y-coordinate. The complex cable configuration has two DOF, and one of them is used for reaching the desired position. It should be noted that the desired position consists of two generalized coordinates, and therefore cannot be exactly reached with one DOF control, but it can be approached.

The desired position gives information about the desired endpoint of each segment. This desired endpoint is given in the Global frame. Thus even if the previous segment makes an error compared to the previous desired position, the current segment will still optimize towards the global desired position. Therefore the position error does not necessarily increase with each segment.

The desired endpoint has another benefit. Together with the desired angle, it gives more information over the track in between the desired points. Without the desired position, the desired angle only gives a hint of where the desired position would be.

Because the instrument is judged on the error that it makes compared to the desired path, a DOF that optimizes towards the desired path is very important.

Increasing error

Whenever a segment is not able to reach the desired end position. The distance between the end point of the current segment and the desired end position of the next segment might be larger. Therefore the next desired position might not be reachable. This can result in an increasing end position error.

Desired angle and desired position

The results show a much better performance from the instrument with complex segments compared to the instrument with simple segments with the same number of DOF. This suggests that the information of the desired

position is more important for the instrument than the information of an angle.

The angle is more important for the starting direction of the next segment than for the current segment. However, the desired position in combination with the desired angle does give an indication of the shape between the desired positions. Therefore, the complex segment seems to be far superior for following different tracks.

The different shapes that a segment is able to make is directly related to the number of DOF it has. Therefore, the different possibilities in shapes of a segment cannot be viewed separately from the DOF of a segment. The larger possibility of shapes from the complex segment might be beneficial in following a path with multiple curves.

Notice that an increase in segments will lead to better results in all the presented cases. This is a direct effect of more information provided to the instrument and an increase of the number of DOF of the instrument.

6.2 Limitations of the model

It should be kept in mind that the algorithm is designed as a tool for comparing the potency of two cable configurations. Although the model tries to be accurate, the results might be inaccurate at sharp bending angles. Therefore, it is not advised to use the model as a path planner, but as an indicator of possibilities.

Notice that the second segment gets a global position that it needs to reach. Just like the mechanical system gets a global position of the preformed track for each of the segments. This gives the instrument the possibility to compensate for the previous errors. Whenever this is not the case, the position error cannot be compensated. This will result in an increasing position error. An increased position error will influence the accuracy of the information provided to the segments. Whenever a desired position is not reached, the instrument lags behind on the desired path. The provided information is based on the previous desired position instead of the end position of the segment. Therefore this information becomes less reliable.

It was decided not to introduce a maximal angle to the instruments. Although the algorithm makes it possible to introduce a maximal bending angle. A maximal angle would be arbitrary. Besides, this arbitrary decision will influence the results. This influence will eventually decrease the amount of information that the results present. Besides, it would also not be realistic to use a constant maximal angle for each segment, because a longer segment might be able to achieve a larger angle. Thus an angle per mm would be more realistic, however, the attachment between different segments will in practice also influence the bending angles.

6.3 In practice

In practice, a third dimension will need to be added to form the needed paths for surgery. However, with the addition of a third dimension, the constant curvature approximation is proven to be less precise [26].

Notice that the number of cables is large in practice. In 3D the minimal number of cables for the simple configuration would be three per segment. Although most of the papers use four cables for this configuration. Whenever diagonal cables are added to the four parallel cables, the total number of cables per segment is eight. A concept with three parallel and three diagonal cables is also an option. Although multiple research groups prefer four cables due to the

intuitive control. The complexity rises with the number of cables. Therefore it is important to optimize towards an instrument with a high maneuverability but a low number of cables.

The friction is neglected in this model. This will directly influence the magnitude of the force applied from the cable. However, because the report is focused on the kinematics rather than the dynamics of the system, the effect on the results will be minimal. Friction can become a problem if the number of segments increases. Notice that the friction will increase with the number of guidance ribs.

Guidance ribs are needed to prevent extreme non-linear behavior. The simple configuration as well as the complex configuration need guidance ribs for larger bending angles. In practice, the instrument might be uncontrollable due to friction if too many guidance ribs are used.

6.4 Design recommendations

Whenever a flexible instrument is designed in combination with the master-slave system, it is recommended to choose for an instrument with a linear curvature. The second DOF is important for the maneuverability of a flexible instrument. Whenever there is chosen to use a flexible instrument with only parallel cables, it is strongly recommended to look at a position based control instead of an angle based control. A combination with the selected master-slave system is inefficient and will demand a large number of segments.

The second recommendation is to look into the manners of providing guidance ribs. Although a higher number of guidance ribs will lead to more linear behavior, a higher number of ribs will also increase the complexity. Therefore it might be interesting to look at other promising ways of guiding the cables like a triple helix structure presented by Henselmans et al. [35].

The third recommendation is to produce an instrument with four or five segments. Although more is always better, a production with five segments seems to be able to cover all the calculated paths, besides each segment makes the instrument more complex. An increasing number of segments would also decrease the length of the segments and might lead to a stiffer instrument, although there is more research needed in this area.

6.5 Future recommendations

There are a couple of recommendations for the improvement of the model. A maximal bending angle can be introduced. Although the code is already capable of using a maximal bending angle, this maximal bending angle should be based on measurements from prototypes. Thus more research is needed to implement a maximal bending angle.

The algorithm only works in two dimensions. A third dimension can be added. This would give more insight into the behavior of the different configurations. However, it should be noted that other papers, like Rucker et al. [26] suggest different out of plane behavior.

The different instruments can be tested on realistic paths. Those paths should be based on the anatomy of the area of interest of the human body.

7. Conclusion

Delft University of Technology has developed two working prototypes of flexible instruments, together with a master-slave system. It was assumed that the instrument with a complex cable configuration requires fewer segments, compared to an instrument with a simple cable configuration, to cover a complex path, with the same accuracy.

The two prototypes were modeled to select the most promising cable configuration. This model was used to predict the kinematic possibilities of those cable configurations. The kinematical shapes are used, in combination with a model of the master-slave system, to judge the configurations on their ability to follow complex paths.

The developed algorithm shows a more accurate performance of the instrument with a complex cable configuration, for the investigated desired paths. In all the investigated paths, the number of needed segments to follow the desired path was lower for the complex cable configuration compared to the simple cable configuration. But, not only the number of segments was lower, the needed number of degrees of freedom, needed to follow a desired path with the same accuracy, was also lower.

The results clearly show that an instrument build from segments capable of forming a shape with a linear curvature has more potential than an instrument existing of segments with a constant curvature. Even when the constant curvature instrument has twice the number of segments and therefore the same number of degrees of freedom.

8. Literature sources

[1] McGee, M. F., Rosen, M. J., Marks, J., Onders, R. P., Chak, A., Faulx, A., V. K. Chen, & Ponsky, J. (2006). A primer on natural orifice transluminal endoscopic surgery: building a new paradigm. *Surgical innovation*, *13*(2), 86-93.

[2] Gammie, J. S., et al. (2010). "Less-invasive mitral valve operations: trends and outcomes from the Society of Thoracic Surgeons Adult Cardiac Surgery Database." The Annals of Thoracic Surgery 90(5): 1401-1410. E1401.

[3] Kang, C. Y., et al. (2012). "Laparoscopic colorectal surgery: a better look into the latest trends." Archives of Surgery 147(8): 724-731.

[4] Diana, M. and J. Marescaux (2015). "Robotic surgery." British Journal of Surgery 102(2): e15-e28.

[5] Wall, J. and J. Marescaux (2011). "Robotic gastrectomy is safe and feasible, but real benefits remain elusive: Comment on “robotic gastrectomy as an oncologically sound alternative to laparoscopic resections for the treatment of early-stage gastric cancers”." Archives of Surgery 146(9): 1092-1092.

[6] Yang Liu, J. L. (2012). "Surgical robotics: A look-back of latest advancement and bio-inspired ways to tackle existing challenges." Frontiers of Mechanical Engineering 7(4): 376-384.

[7] Marcus, H., et al. (2013). "Surgical robotics through a keyhole: from today's translational barriers to tomorrow's “disappearing” robots." Biomedical Engineering, IEEE Transactions on 60(3): 674-681.

[8] Tevlin, R., et al. (2015). "Impact of surgical innovation on tissue repair in the surgical patient." British Journal of Surgery 102(2): e41-e55.

[9] Hughes-Hallett, A., et al. (2015). "Quantitative analysis of technological innovation in minimally invasive surgery." British Journal of Surgery 102(2): e151-e157.

[10] Landry, C. S., et al. (2010). "Bilateral robotic-assisted transaxillary surgery." Archives of Surgery 145(8): 717-720.

[11] Khanna, A. K. and R. Khanna (2011). "Future of Surgery and Shrinking Surgeon." Indian Journal of Surgery 73(2): 87-89.

[12] Burgner-Kahrs, J., et al. (2015). "Continuum Robots for Medical Applications: A Survey." Robotics, IEEE Transactions on 31(6): 1261-1280.

[13] Burgner, J., Swaney, P. J., Rucker, D. C., Gilbert, H. B., Nill, S. T., Russell, P. T., & Webster, R. J. (2011). A bimanual teleoperated system for endonasal skull base surgery. In *Intelligent Robots and Systems (IROS), 2011 IEEE/RSJ International Conference on* (pp. 2517-2523). IEEE.

[14] Gerboni, G., Henselmans, P. W., Arkenbout, E. A., van Furth, W. R., & Breedveld, P. (2015). HelixFlex: bioinspired maneuverable instrument for skull base surgery. Bioinspiration & biomimetics, 10(6), 066013.

[15] Ota, T., Degani, A., Schwartzman, D., Zubiate, B., McGarvey, J., Choset, H., & Zenati, M. A. (2009). A highly articulated robotic surgical system for minimally invasive surgery. *The Annals of thoracic surgery*, *87*(4), 1253-1256.

[16] Received from Henselmans. P.

[17] Breedveld, P. (n.d.). Retrieved November 22, 2017, from https://www.bitegroup.nl/category/maneuverable-devices/multiflex/

[18] Chirikjian, G. S., & Burdick, J. W. (1990, May). An obstacle avoidance algorithm for hyper-redundant manipulators. In *Robotics and Automation, 1990. Proceedings., 1990 IEEE International Conference on* (pp. 625-631). IEEE.

[19] H. Choset, W. Henning, A follow-the-leader approach to serpentine robot motion planning, J. Aerosp. Eng. 12 (2) (1999) 65–73.

[20] Maciejewski, A. A., & Klein, C. A. (1985). Obstacle avoidance for kinematically redundant manipulators in dynamically varying environments. *The international journal of robotics research*, *4*(3), 109-117

[21] Godage, I. S., Branson, D. T., Guglielmino, E., & Caldwell, D. G. (2012, August). Path planning for multisection continuum arms. In *Mechatronics and Automation (ICMA), 2012 International Conference on* (pp. 1208-1213). IEEE.

[22] Henselmans, P.W.J. (2013). Modeling and design of a helix-cable actuated steerable instrument for minimally invasive surgery (MSc thesis).

[23] Hibbeler, Russell C. Engineering Mechanics: Statics. Pearson,2008.

[24] CES Edupack 2017 (Granta Design Limited, 2017)

[25] Webster III, R. J., & Jones, B. A. (2010). Design and kinematic modeling of constant curvature continuum robots: A review. *The International Journal of Robotics Research*, *29*(13), 1661-1683.

[26] Rucker, D. C., & Webster III, R. J. (2011). Statics and dynamics of continuum robots with general tendon routing and external loading. *IEEE Transactions on Robotics*, *27*(6), 1033-1044.

[27] P. E. Dupont, J. Lock, B. Itkowitz, and E. Butler (2010). Design and control of concentric tube robots. IEEE Transactions on Robotics, (In Press).

[28] Rucker, D. Caleb, and Robert J. Webster III (2014). "Mechanics of continuum robots with external loading and general tendon routing." *Experimental Robotics*. Springer Berlin Heidelberg.

[29] C. Li and C. Rahn (2002). Design of continuous backbone, cable-driven robots. ASME Journal of Mechanical Design, 124(2):265–271, doi:10.1115/1.1447546.

[30] Gravagne, I. A. and Walker, I. D. (2002). Manipulability, force, and compliance analysis for planar continuum robots. IEEE Transactions on Robotics and Automation, 18(3): 263–273.

[31] Immega, G. and Antonelli, K. (1995). The KSI tentacle manipulator. IEEE International Conference on Robotics and Automation, Vol. 3, pp. 3149–3154.

[32] Cies´lak, R. and Morecki, A. (1999). Elephant trunk type elastic manipulator–a tool for bulk and liquid materials transportation. Robotica, 17(1): 11–16.

[33] Hannan, M. W. and Walker, I. D. (2003). Kinematics and the implementation of an elephant's trunk manipulator and other continuum style robots. Journal of Robotic Systems, 20(2): 45–63.

[34] Jones, B. A. and Walker, I. D. (2006). Practical kinematics for real-time implementation of continuum robots. IEEE Transactions on Robotics, 22(6): 1087–1099.

[35] Henselmans, P.W.J. (2018) Concept phase: A New Mechanical Approach for Follow-the-Leader propagation of a Flexible Surgical Instrument.

[36] Levien, R. (2008). The Euler spiral: a mathematical history. Rapp. tech.